Electrical and [illegible]
Engineering

Efficient Optical Logic, Interconnections and [illegible]ng Using Quantum Confined Structures

[illegible] ANNUAL REPORT

[illegible] Investigator

and [illegible] Investigator

[illegible] and R. [illegible] Yan

[illegible] Barron

Graduate Student Researchers

[illegible] Visiting Research Engineer

C.I. Technical Report #91-11

UNIVERSITY OF
SANTA BARBARA

Efficient Optical Logic, Interconnections and Processing Using Quantum Confined Structures

AFOSR #89-0549 - ANNUAL REPORT

9/30/89 - 3/31/91

by

L.A. Coldren: Principal Investigator

A.C. Gossard: Co-Principal Investigator

K.J. Simes and R.H. Yan:

(former) Graduate Researchers

K.K. Law and C.C. Barron:

Graduate Student Researchers

M. Whitehead: Visiting Research Engineer

ECE Technical Report #91-11

Department of Electrical & Computer Engineering

University of California at Santa Barbara

May 1991

REPORT DOCUMENTATION PAGE

Form Approved
OMB No. 0704-0188

1. AGENCY USE ONLY (Leave blank)	2. REPORT DATE	3. REPORT TYPE AND DATES COVERED
	May 91	Annual Report 9/30/89-3/31/91

4. TITLE AND SUBTITLE
Efficient Optical Logic, Interconnections and Processing Using Quantum Confined Structures

5. FUNDING NUMBERS
AFOSR-89-0549

6. AUTHOR(S)
Professors L. A. Coldren & A. C. Gossard

7. PERFORMING ORGANIZATION NAME(S) AND ADDRESS(ES)
University of California
Santa Barbara, CA 93106

8. PERFORMING ORGANIZATION REPORT NUMBER
AFOSR-TR- 91 0662

9. SPONSORING/MONITORING AGENCY NAME(S) AND ADDRESS(ES)
AFOSR/NE
Bldg 410
Bolling AFB DC 20332-6448
Alan Craig

10. SPONSORING/MONITORING AGENCY REPORT NUMBER
2305/B4

11. SUPPLEMENTARY NOTES

12a. DISTRIBUTION/AVAILABILITY STATEMENT
UNLIMITED

12b. DISTRIBUTION CODE

13. ABSTRACT (Maximum 200 words)

This report describes our work for the period of 1 May 89 to 31 Mar 91. The work has been strongly focused on the development of high-efficiency surface-normal Fabry-Perot cavity modulators, in particular the asymmetric Fabry-Perot modulator (AFPM). In contrast to the hihg-finesse, refractive index-tuned, symmetric cavity type of modulator (SFPM), on which we first reported under contract #85-0323, the AFPM utilizes the electroabsorptive properties of the intra-cavity medium - normally a GaAs-AlGaAs multiple quantum well structure - to balance the initially unbalanced (asymmetric) mirrors of a low-finessee cavity, thus making it possible to achieve high contrast ratio, very efficient transfer function with low operating voltage, low insertion loss and, importantly, significantly wider optical bandwidth for the SFPM. During this period we made one of the initial demonstrations of the AFPM, where we achieved a contrast ratio of 22:1 in (see back)

14. SUBJECT TERMS

15. NUMBER OF PAGES

16. PRICE CODE

17. SECURITY CLASSIFICATION OF REPORT	18. SECURITY CLASSIFICATION OF THIS PAGE	19. SECURITY CLASSIFICATION OF ABSTRACT	20. LIMITATION OF ABSTRACT
UNCLASSIFIED	UNCLASSIFIED	UNCLASSIFIED	UL

in reflection, at a d.c operating voltage of IIV, and with only 3.7dB insertion loss.

TABLE OF CONTENTS

I. INTRODUCTION
- 1. Summary of Work
- 2. Overview of Experimental Work on Transverse Electro-Optic Modulators

II. SYMMETRIC (ELECTRO-REFRACTIVE) FABRY-PEROT MODULATORS (SFPMs)
- 1. Review of Operating Principles
- 2. Performance of SFPMs

III. ASYMMETRIC (ELECTROABSORPTIVE) FABRY-PEROT MODULATORS (AFPMs)
- 1. Principles of AFPM Device Operation
- 2. Initial Demonstration of AFPM with High Contrast
- 3. Low Voltage Design with Record Modulation Transfer Function
- 4. Optimization of the AFPM
- 5. Comparison of Various FP Modulators
- 6. Sensitivity Analysis of AFPMs
- 7. Superlattice AFPM with a Normally-Off Characteristic
- 8. Superlattice AFPM Self-Electro-Optic-Effect Device

IV. HIGH FREQUENCY OPERATION OF FP MODULATORS
- 1. Device Structure and Fabrication
- 2. Electrical Characterization
- 3. Small-Signal Modulation Results
- 4. Prospects for Higher Frequency Modulation

V. Conference and Journal Publications

VI. Personnel

I. INTRODUCTION

I.1 Summary of Work

This report describes our work for the period 1 May 1989 to 31 March 1991. The work has been strongly focused on the development of high-efficiency surface-normal Fabry-Perot cavity modulators, in particular the *asymmetric Fabry-Perot modulator* (AFPM). In contrast to the high-finesse, refractive index-tuned, symmetric cavity type of modulator (SFPM), on which we first reported under contract #85-0323, the AFPM utilizes the electroabsorptive properties of the intra-cavity medium - normally a GaAs-AlGaAs multiple quantum well structure - to balance the initially unbalanced (asymmetric) mirrors of a low-finesse cavity, thus making it possible to achieve high-contrast ratio, very efficient transfer function with low operating voltage, low insertion loss and, importantly, significantly wider optical bandwidth than for the SFPM. During this period we made one of the initial demonstrations of the AFPM, where we achieved a contrast ratio of 22:1 in reflection, at a d.c. operating voltage of 11V, and with only 3.7dB insertion loss.

After these encouraging results our efforts were directed towards optimizing the AFPM performance, particularly reduction of the operating voltage, whilst maintaining high optical efficiency. By reducing the thickness of the device active region, and increasing the finesse of the cavity to compensate, we were able to demonstrate a record reflection transfer function of more than 20% per volt, i.e. 47% ΔR for only 2V bias swing, and a peak contrast ratio of $\approx$70:1 with 3V swing. Together with the experimental work, we have simultaneously carried out a theoretical optimization of the AFPM and an analysis of its tolerance to variations in such parameters as operating wavelength, voltage swing, cavity thickness and operating temperature.

Using the blue shift of the absorption edge in a superlattice (SL) structure (Field-Induced Stark Localization), which we made the first observation of under contract #85-0323, we have also demonstrated the first normally-off AFPM, i.e. where the device reflectivity is increased from a low value (off state) as increasing reverse bias is applied. With this characteristic the device is capable of operating as a SEED (self electro-optic effect device - a type of optoelectronic switch), and we have duly demonstrated an SL-AFPM-based SEED, with the highest on:off ratio ever reported (> 100:1).

Whilst shifting emphasis toward the AFPM during this period, the SFPM has still been under investigation. We have succeeded in reducing the operating voltage and improving the contrast whilst assessing the limits on efficient modulation. SFPM devices suitable for high frequency measurements have been fabricated and shown to have up to ≈ 6 GHz bandwidth - an RC limitation determined by the device size. In the near future we expect to have an improved fabrication process, allowing reduced device dimensions and bandwidths in the 10s of GHz range.

Current work is still aimed at device efficiency optimization. There is some desire to see a voltage swing compatible with ECL for high-speed optical interconnects. We have begun to investigate wider quantum well widths (with greater field sensitivity of QCSE, and less sensitivity to well width fluctuations) for the device active region, and the reduction of barrier width, in order to maximize the absorption change for a given applied voltage.

I.2 Experimental Work on Tranverse Electro-Optic Modulators

Highly efficient electro-absorption and electro-refraction effects in semiconductor multiple quantum wells and superlattices, along with increased system demands have advanced high-performance optical modulators which can be used in various applications: as an intra-laser-cavity controlling device, transmitter of telecommunications including interconnections for integrated circuits, and optical information processing. Among various design issues for practical applications, one of the important considerations is low drive power, e.g. low operating voltage swing in electro-optic modulators. Waveguide (in-plane) devices tend to provide low drive voltages (≈1 volt) because the field is applied perpendicular to the light propagation direction [1]; however, the coupling of the light into the waveguide adds complexity to practical implementations. On the other hand, although coupling is relatively easy, surface-normal (transverse) devices tend to require high drive voltages (>10 volts) due to short interaction lengths [1].

Another important device parameter is the amount of electrical input power that is modulated onto the optical output power. Using as a figure-of-merit the normalized electro-optic transfer function (M_v) [2], defined as the percentage modulation of the input light per unit driving voltage, to relate the transfer function of electro-optic modulators between the electrical and optical signals, it can be seen that previous transverse modulators have M_v's of ≤ 8 %/V, and efficient waveguide modulators have a representative value of < 15 %/V [1].

Figure I.1 briefly summarizes the performances of various transverse modulators in terms of required voltage swing, reflectivity (or transmission) change, and contrast ratio between on and off states. Basic structures of the listed devices are also shown in the inset, although details can be found in the cited references. Dashed lines represent various normalized transfer functions. Due to the large excitonic absorption strength of the quantum confined Stark effect (QCSE), all devices except one use multiple quantum wells (MQWs) as the electro-optic medium. As indicated, one of the closed-square points (■) represents an asymmetric Fabry-Perot (AFP) modulator using the Wannier-Stark localization effect of superlattices [3].

The first demonstration of transverse modulators by Wood et al. [1] in 1985 employed a simple PIN-MQW transmission configuration with the QCSE. Although more than 30% transmission has been obtained with only 8 volts, the contrast ratios are quite limited (≤ 3 dB).

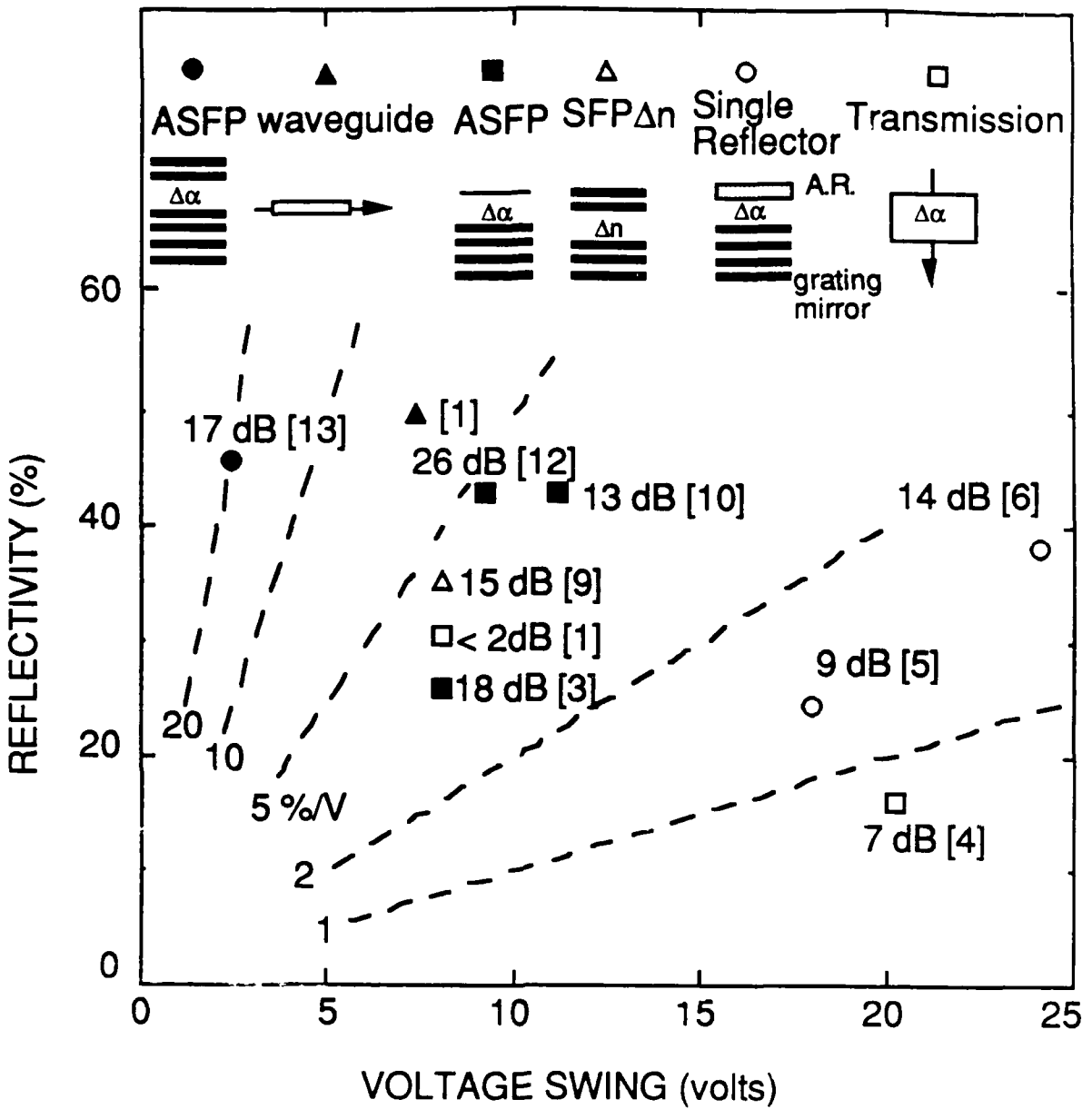

Figure I.1

A performance comparison of various transverse modulators. The schematic structures of the devices are shown in the inset on the top. The dashed line represents different normalized transfer function from 1 to 20 %/V. The numbers are the contrast ratios [references]. The average waveguide performance is also included for reference.

Key to reference sources: □:([1,4]); ○ :([5,6]); ■:([3,10,12]); ▲:([1]); △ :([9]); ●:([13]).

Using the simple transmission configuration, the contrast ratio has been improved to ≈7 dB [4] by using a much thicker active region, but the required voltage increases and therefore M_v decreases. By incorporating a single reflector (monolithically grown quarter-wavelength stack, or deposited-metal) on one side of the active region and an anti-reflection layer on the other side, the effective interaction length is doubled from the simple transmission configuration [5,6]. Both the contrast and the transfer function are doubled for the same voltage swing. As seen from Figure I.1, M_v increases from 0.8 to 1.5 %/V due to the addition of the reflector. Such an advance has very important implications. With our in-house MBE growth facility, layers of thickness on the order of a quarter-wavelength can be deposited with great accuracy. Therefore, in addition to quantum-confined structures for electrons, we are also able to grow multi-layer quarter-wave stack mirrors with which to confine the optical energy. This enhances the interaction between the electronic and the optical waves without increasing the physical length of the device.

Using two reflectors to form a Fabry-Perot (FP) cavity [7,8], the interaction length can be increased even more, and the amount of enhancement depends on the *finesse* given by the mirror reflectivities [9]. Although the introduction of FP structures places a limit on the optical bandwidth, BW_o (see Fig. III.11), over which the device can be operated, the required voltage swing is greatly reduced. Therefore, as long as BW_o remains large enough, e.g., no less than the room temperature linewidth of quantum well heavy hole exciton absorption peak, the use of FP structures to improve the performance is justified.

Both electro-refraction [7,8] and electro-absorption [10] effects can be used with FP structures. To use the electro-refraction effect, the mirror reflectivities on both sides of the FP cavity are designed to be the same (index-tuned symmetric FP or SFPΔn), and the index change is used to tune the FP mode to achieve the modulation. Depending on the operating wavelength, the device can be normally-on (reflecting with no bias) or normally-off (reflecting with bias). As much as 4 %/V has been achieved with contrast ratios more than 15 dB [9]. However, due to relatively large *finesse*, BW_o is quite limited (≈ 5Å).

Although both electro-absorption and electro-refraction effects can be used with multiple quantum wells (MQWs), the electro-refraction effect should be used at a wavelength that is away from the sharp excitonic absorption edge, in order to avoid any induced absorption change and to lose the advantages of sharp excitonic features [11]. Since both effects are

reduced with separation from the exciton, it is generally true that MQWs work more efficiently in the *electro-absorption* mode than in the *electro-refraction* mode; that is, FPs with an absorption change ($\Delta\alpha$) tend to operate with lower voltages than the SFPΔn, or for the same voltage, they have wider BW_o. However, SFPΔn devices switch the light instead of absorbing it, and such an operating mode can be quite useful for photonic switching and communication applications in which one wishes to preserve the optical energy. We report some of our more recent results for SFPΔn modulators in Sections II & IV.

Unequal mirrors are used with electro-absorption effects to implement asymmetric Fabry-Perot (AFP) modulators [11,12]. The modulation mechanism is as follows. Without cavity loss, the overall reflectivity is quite high if the bottom mirror reflectivity is made close to unity and the top mirror reflectivity is significantly less. With applied fields, the increased cavity loss reduces the effective reflectivity from the bottom mirror at the top surface, and the overall reflectivity can be made zero when the effective reflectivity from the bottom has an equal magnitude to the top mirror reflectivity, yielding the off state. The first experiments with AFPs simply used the semiconductor-air interface as the top mirror [10,12], and comparable M_v's are obtained with significantly wider BW_o's ($\geq$3 nm) than for SFPΔn's.

More importantly, when a $\approx$ 75% reflectivity top mirror is used, a voltage swing as low as 2 volts is enough to change the device reflectivity by more than 40 %, i.e. > 20 %/V [13]. Such an M_v represents the-state-of-the-art in transverse modulator performance, and we will discuss such a device family using asymmetric Fabry-Perot structures in more detail in this report.

II. Symmetric (Electrorefractive) Fabry-Perot Modulators (SFPMs)

II.1. Review of Operating Principles

As we explained in our last report, the intent behind incorporating a Fabry-Perot étalon into a MQW electrooptic modulator is to increase the interaction length between the active material and the light beam, as compared to simple transmission or double-pass reflection designs [4–6]. Modulation is achieved by modifying the shape of a Fabry-Perot cavity resonance with an electric field. We began our work on Fabry-Perot modulators by concentrating on modulation of the refractive index in high-finesse structures, which phase shifts the cavity resonance. This is shown below schematically in Fig. II.1. Since then our attention has shifted to low-finesse asymmetric FPMs, which offer the advantage of increased optical bandwidth (see Section III). For some applications, however, such as a four-port optical switch, which requires the modulator to operate simultaneously in transmission and reflection, the symmetric version retains its appeal.

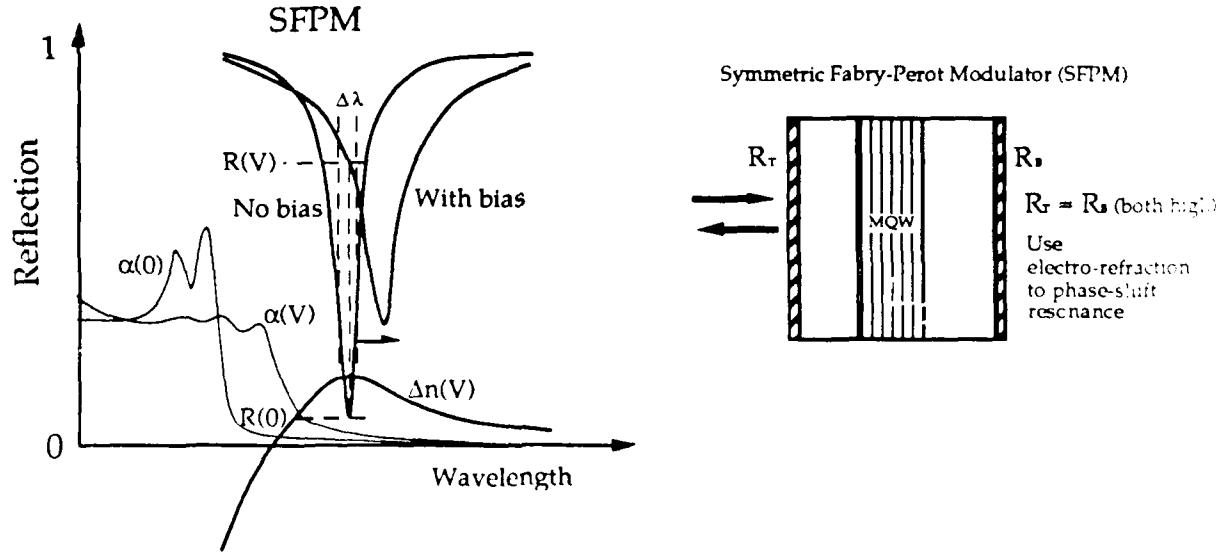

Figure II-1.

Efficient modulation in a high-finesse FP cavity is effected by shifting the cavity resonance through electrorefraction.

II.2. Performance of SFPMs

In our last report we presented measurements of a symmetric MQW FP modulator with a contrast ratio of ≈10:1 for drive voltages as low as 7 V. Since then, we have grown and characterized similar modulators with contrast ratios as high as 30:1 with an 8 V bias.[9] The device performance (contrast ratio, insertion loss, drive voltage) depends largely on the placement of the FP resonance, which is determined by the exact cavity length. To illustrate the effect of resonance placement relative to the exciton wavelength, we present here measurements of two SFPMs fabricated from the same MBE-grown wafer. The device structure consists of a 9-period front mirror and a 12.5-period back mirror, with a nominally 0.75 μm layer of MQW material (100Å GaAs/100Å $Al_{0.2}Ga_{0.8}As$). We intentionally refrained from rotating the wafer during growth of the active region in order to produce devices with a range of operating wavelengths. The structure is shown schematically below.

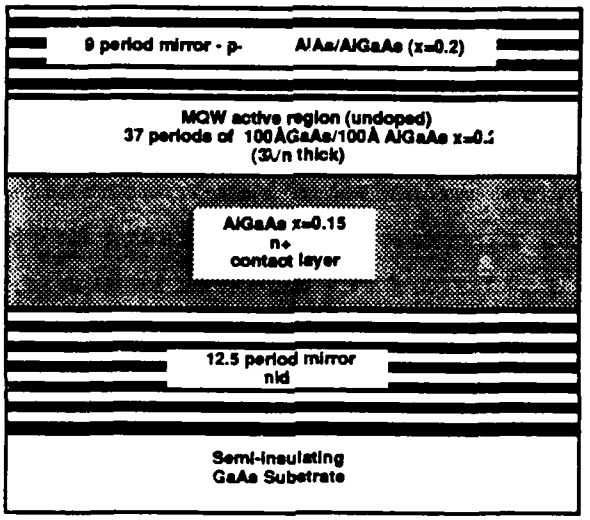

Figure II.2

A schematic of the reduced voltage/improved contrast SFPM structure for which data are presented on the following pages.

The effect of operating with the FP resonance at two different wavelengths relative to the MQW absorption edge is illustrated in Figures II.3-II.6. Device "FP8D9", for example, has the operating wavelength at ≈ 857nm and 7.8 nm separation between the FP resonance and the heavy hole exciton, while device "FP8E1" has its FP resonance at ≈ 878nm and a $\Delta_{FP/exciton}$ of 25nm.

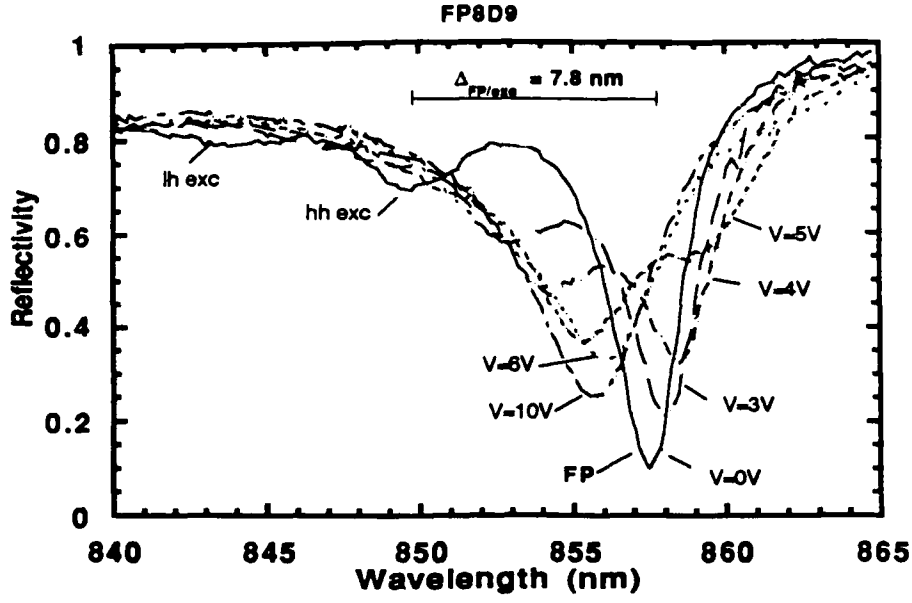

Figure II.3

Measured reflection spectra, obtained using microscope-based system, for a FP structure with 9-period top mirror, 12.5-period bottom mirror and 3λ/n-thick MQW active medium. The wavelength separation between the FP resonance and the excitonic heavy-hole absorption, $\Delta_{FP/exc}$, is 7.8nm in this case.

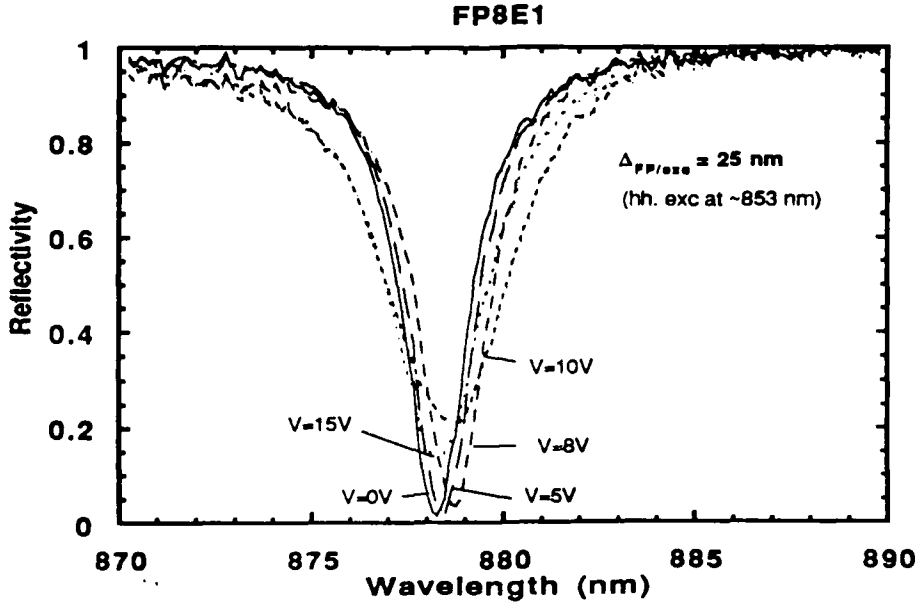

Figure II.4

Measured reflection spectra, obtained using microscope-based system, for a FP structure with 9-period top mirror, 12.5-period bottom mirror and 3λ/n-thick MQW active medium. The wavelength separation between the FP resonance and the excitonic heavy-hole absorption, $\Delta_{FP/exc}$, is 25nm in this case.

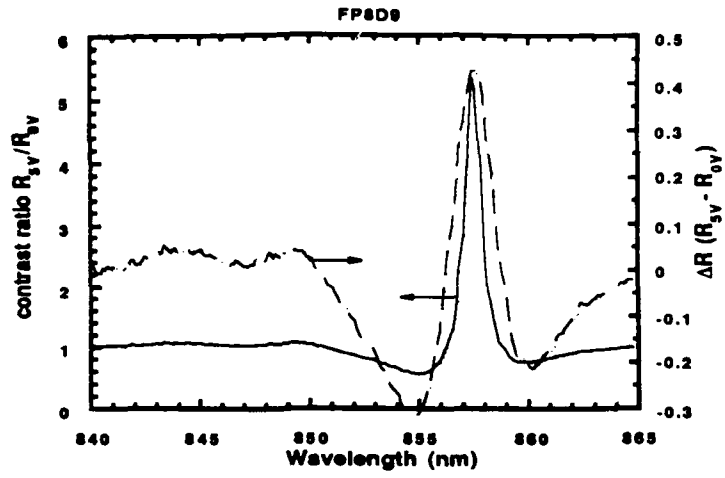

Figure II.5

Contrast ratio and ΔR vs V for MQW-based active structure used for data of Fig. II.3. The bias is changed from 0V to 5 V. The FP mode is quite close to the exciton absorption edge ($\Delta_{FP/exc}$ = 9.9 nm), and there is some absorption at zero field, causing the reflection at the FP resonance to be non-zero; the contrast ratio is thus reduced. The FP mode shift at lower fields is accentuated and the voltage required to for a high ΔR is reduced.

The data in Fig. II.5 show that a device such as "FP8D9" which operates relatively close to the absorption edge requires less bias to shift the FP resonance, and has lower insertion loss, but also has limited contrast because of its higher zero-field absorption. Operating relatively far away from the absorption edge (device "FP8E1", Fig. II.6) increases the potential contrast but also increases the drive voltage and insertion loss.

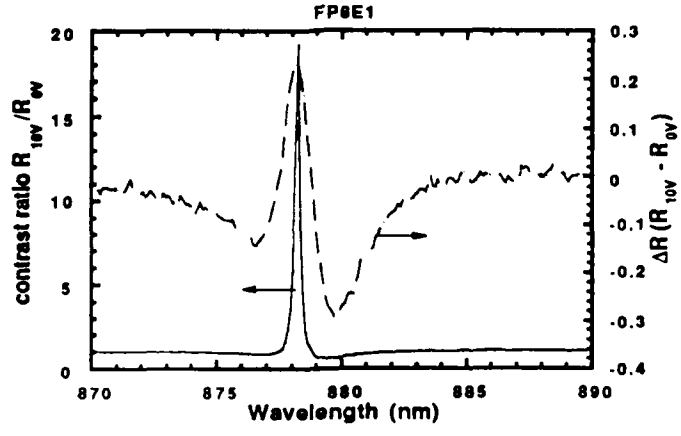

Figure II.6

Contrast ratio and ΔR vs V for MQW-based active structure used for data of Fig. II.4. The bias is changed from 0V to 10 V. $\Delta_{FP/exc}$ is higher for this sample; thus it takes more voltage to shift the resonance. The FP mode dips quite sharply to zero, making the contrast ratio high.

III. Asymmetric (Electroabsorptive) Fabry-Perot Modulators (AFPMs)

III.1 AFPM Operating Principles

A Fabry-Perot structure with MQW as the active material can either operate with electro-absorption or electro-refraction effects by designing the Fabry-Perot mode to locate closer to or further away from the excitons. The latter mode of operation has been described in detail in Ref. [9] where the mirrors on both sides of the cavity are made symmetric, i.e. equally reflective. To make use of the electro-absorption effect, the Fabry-Perot cavity can be symmetric or asymmetric. As will be discussed later in Section III.5, the asymmetric FP (AFP) structure [10,12] is found to be the more efficient structure for low voltage operation.

The top (bottom) mirror of an AFP structure has an amplitude reflection coefficient of $r_{t(b)}$ and power reflectivity of $R_{T(B)}=|r_{t(b)}|^2$, viewed from the cavity. And $R_B>R_T$ is used in the design. The transmission coefficient of the top mirror is t_t. As the input light with an electric field amplitude of a_i is incident upon the top surface, the top mirror reflects a portion the input field of an amplitude

$$a_{ot} = - r_t a_i \qquad (1)$$

where the reflection from the top mirror viewed from the surface, $-r_t$ is in the opposite phase of the reflection viewed from the cavity, r_t. We choose a reference plane so that $r_t>0$. With this choice of reference plane, the transmission coefficient t_t is a real number [14]. The total reflection in amplitude from the bottom mirror is the sum of all possible multiple reflections:

$$a_{ob} = \sum_{m=1}^{\infty} a_{obm} = (t_t)^2 \left[(r_b \exp(-\alpha l)) + \cdots + (r_b \exp(-\alpha l))(r_t r_b \exp(-\alpha l))^{m-1} + \cdots\right] a_i$$

$$= \frac{(t_t)^2 r_b \exp(-\alpha l)}{1 - r_t r_b \exp(-\alpha l)} a_i \qquad (2)$$

where α is the absorption coefficient in the cavity. We show various reflected components schematically in Figure III.1 (a) and (b) for the case of $\alpha=0$ and $\alpha=\ln(r_b/r_t)$, respectively. Adding (1) and (2), we obtain the total amplitude reflection r_{total} as:

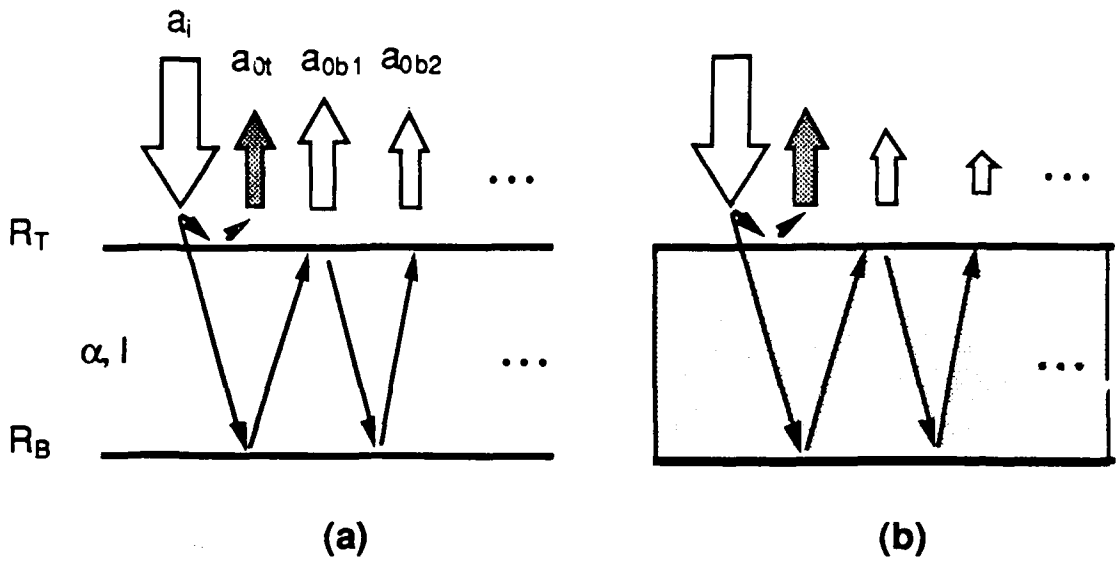

Figure III.1

Schematic drawing of the operating principle for asymmetric Fabry-Perot absorption modulator: (a) low loss, and (b) high loss.

$$r_{total} = \frac{a_{ot} + \sum_{m=1}^{\infty} a_{obm}}{a_i}$$

$$= \frac{- r_t + r_b \exp(-\alpha l)}{1 - r_t r_b \exp(-\alpha l)} \qquad (3)$$

where we have assumed the top mirror is lossless, i.e. $|r_t|^2+|t_t|^2=1$. Very importantly, we have $r_{total}=0$ when the condition of Figure III.1(b) (i.e., $\alpha=\ln(r_b/r_t)$) is satisfied. Note that in this case, $a_{ob}/a_i = - a_t/a_i$. On the other hand, r_{total} remains quite large when $\alpha=0$ as in Figure III.1(a), where $a_{ob}/a_i > - a_t/a_i$.

Written in terms of the power reflectivity, $R_{FP}=|r_{total}|^2$ is given as

$$R_{FP} = \frac{|\sqrt{R_T} - \sqrt{R_B}\exp(-\alpha l)|^2}{|1 - \sqrt{R_T R_B}\exp(-\alpha l)|^2} \qquad (4)$$

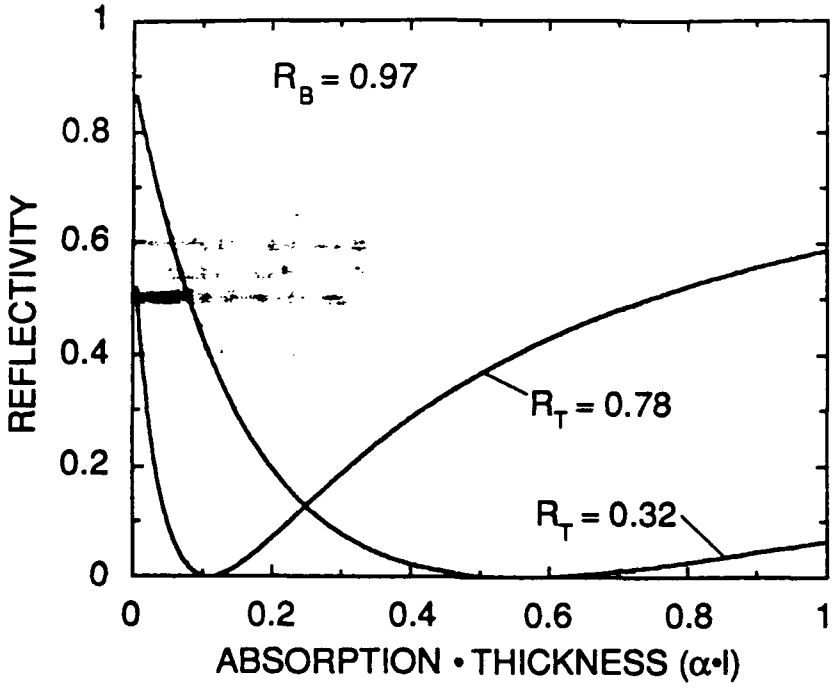

Figure III.2

Reflectivity of the AFP as a function of the cavity loss and cavity length product for top mirror reflectivity of 0.32 and 0.78.

Assuming R_B=0.97, Figure III.2 plots R_{FP} as a function of $\alpha \cdot l$ for two different R_T's. In the experiments described in the next section, we use a quarter wavelength stack of $Al_{0.2}Ga_{0.8}As$ and AlAs as the top mirror, and the available mirror reflectivities are discrete from 0.32 to 0.78 as the number of period increases from 0 to 5. As the loss in the cavity changes, the overall reflectivity of the Fabry-Perot structure is modulated. For example, when $\alpha \cdot l$ changes from 0.02 to 0.11, the reflectivity changes from 50 % (on) to 0 % (off) with R_T=0.78. This is the basic operating principle of AFP modulators. Depending on whether the absorption increases (e.g. QCSE) or decreases (Wannier-Stark localization) as the field increases, the device at zero bias can be either on (normally-on) or off (normally-off) [15]. The fact that

$$R_B \exp(-2\alpha l) = R_T \qquad (5)$$

makes R_{FP} zero is the most interesting property of the AFP modulators. Conventional

absorption modulators can make the device reflectivity arbitrarily small but not absolutely zero [1]. By designing R_T smaller than R_B, the (field-induced) absorption makes the effective reflectivity from the bottom mirror through the cavity loss equal to R_T but opposite in phase so that the net reflectivity equal zero. Since the bandwidth is determined by the resonance width at the off-level, the bandwidth of the AFP is generally wider than high-*finesse* Fabry-Perots that use index modulation, due to its less reflective mirrors at resonance.
In following sections, we show two interesting examples of AFP modulators. The first one uses an air-semiconductor interface as the top mirror. The second one uses a more optimized structure to achieve an extremely low drive voltage.

III.2. Initial Demonstration of AFPM with High Contrast

The AFP is composed of a pair of asymmetric mirrors separated by an active spacer layer. The front end is made less reflective than the bottom grating. In the orignal demonstration, the top mirror was simply an air-semiconductor interface [12]. The advantage of no grating mirror on top is to avoid the extra resistivity due to multiple heterojunctions, although graded junctions can reduce the resistivity [16].

The structure shown in Figure III.3(a) is grown by molecular beam epitaxy. The bottom mirror, with a theoretical reflectivity of R_B=97 %, was made of $15^1/_2$ periods of alternating 725 Å AlAs and 625 Å $Al_{0.2}Ga_{0.8}As$ layers doped with Si to $\approx 10^{18}$ cm^{-3} grown on an n^+-GaAs substrate. The active region has $70^1/_2$ periods of undoped 100 Å GaAs/100 Å $Al_{0.2}Ga_{0.8}As$ multiple quantum wells (MQW). The top layer is a Be-doped $\approx 10^{18}$ cm^{-3} $Al_{0.1}Ga_{0.9}As$ layer, $\approx$ 0.55 μm thick. Further details are can be found in Ref. [10].

Figure III.3(b) shows a broad-band spectrum of the AFP epitaxial structure without bias. The apparent stop band width is narrower than that of the grating mirror, due to the absorption of the active region for wavelengths shorter than ~860 nm. The exciton position is also marked (determined from the narrow band spectrum, discussed below). We did not rotate the wafer during the growth of the active region and the top layer to provide a slight taper in thickness over the wafer. In this particular sample, the center resonant mode is around 863 nm, which is the design value with the refractive index taken from Ref. [17]. We have modeled the refractive index of the MQW region as given by that of AlGaAs with the Al composition taken

as the averaged value of the MQW, 0.1. The mode position in monolithically-grown Fabry-Perot structures depends on the cavity length as well as the refractive index. Therefore, the control of thickness and composition, and a knowledge of refractive indices are important for such structures.

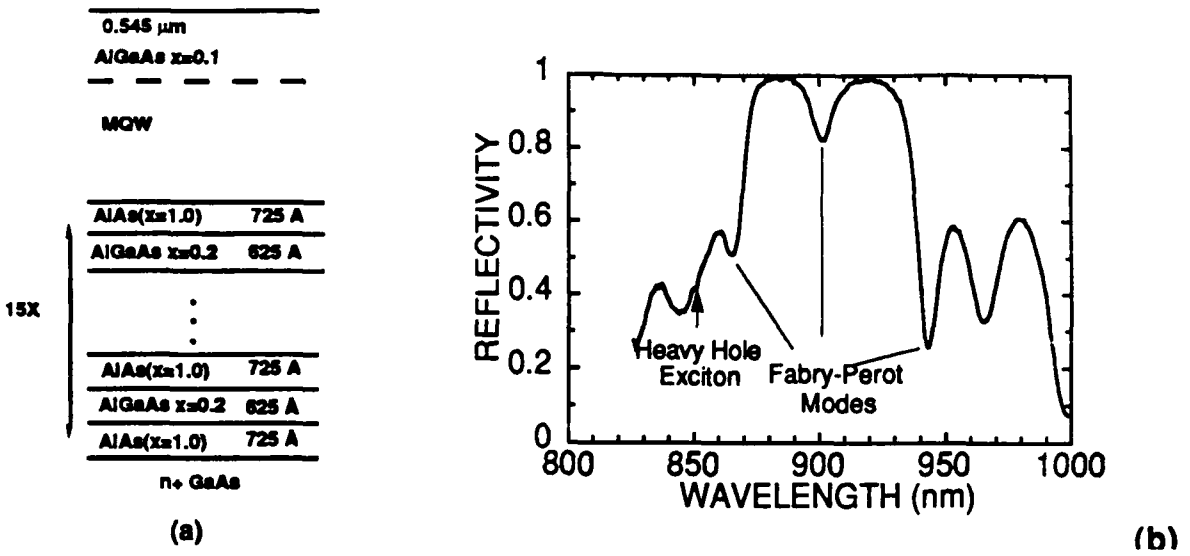

Figure III.3

(a) Layer structure used in our initial demonstration of the AFPM. See text for doping details.

(b) Broad-band spectrum without bias for the structure shown in (a). The reflectivity is relative to that of a gold mirror (R_{max} ≈ 98%). The heavy hole exciton position as well as the Fabry-Perot modes are indicated.

Shown in Figure III.4(a) are the narrow band spectra for reverse bias voltages of 0, 4, 8, and 11 volts for the same device as in Figure III.3. The shift of the exciton with electric field is clearly observed. The positions of the excitons and the Fabry-Perot modes are indicated by the voltage labels and the dotted curve, respectively. The exciton moves from 850 to 853, 857 and 860 nm, as the field increases from 10 (built-in field) to 40, 70 and 90 kV/cm, respectively. The result of the exciton shift is an increase of absorption at the resonant wavelength from ≈ 600 cm^{-1} to ≈ 4000 cm^{-1}. The amount of absorption can be roughly estimated from the calculated reflectivity at resonance, as shown in Figure III.2 with R_T=0.32. Small shifts of the FP mode are also observable. In this sample the exciton coincides with the FP mode at the desired loss of ~4000 cm^{-1} where the reflectivity becomes very low (≤ 2 %). This results in a fairly wide bandwidth. The on/off ratio between 0 and 11 volts is shown in Figure III.4(b) as a function of wavelength. By defining the bandwidth as the range over which the contrast ratio

is greater than 10, we have obtained a bandwidth of 3.4 nm. The same bandwidth will be obtained if the bandwidth is defined in terms of the reflectivity in the off-state being smaller than 5%, because the insertion loss is about 3-4 dB. In the center of the bandwidth, the peak contrast ratio is 22 with an insertion loss of 3.7 dB. At the edge of this range where the contrast is 10 the insertion loss is as low as 2.8 dB.

Figure III.4

(a) Narrow band spectra for reverse bias voltages of 0, 4, 8, and 11 volts for the same device structure as in Figure III.3. The positions of the excitons and the Fabry-Perot modes are indicated by the voltage labels and the dotted line, respectively.

(b) The on/off ratio between 0 and 11 volts as a function of wavelength. By defining the bandwidth as the range over which the contrast ratio is greater than 10, we have obtained a bandwidth of 3.4 nm.

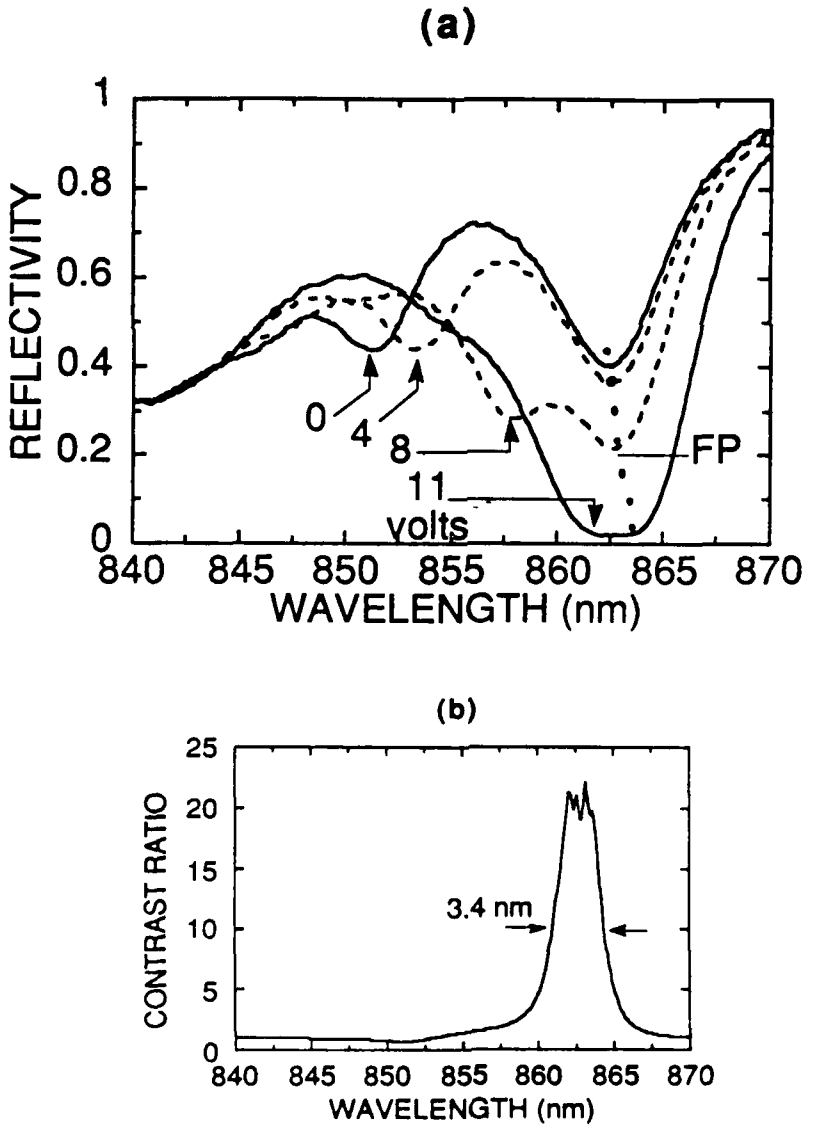

When the exciton coincides with the FP mode, the resonance shape (reflectivity spectrum) is far from Lorentzian but more like rectangular. This is due to the refractive index shift associated with the exciton. Large positive (negative) index changes (≈ 1%) are expected to appear on the longer (shorter) wavelength side of the exciton (now also FP mode), and these index changes widen the FP mode. This "mode pushing" effect effectively increases the optical bandwidth, as indicated later in Fig. III.11

III.3 Low-Voltage Design with Record Modulation Transfer Function

Normally-on operation in the AFP modulator is achieved by using a pair of asymmetric mirrors separated by a low loss active spacer layer to make the net reflectivity at the resonant wavelength high at zero bias. The off-level is provided by increasing the loss (e.g., electro-absorption effect) in the cavity so that the effective reflection from the bottom grating viewed through the lossy cavity cancels the reflection from the front end, as discussed above. Increasing the front reflection could decrease the required amount of absorption and active layer thickness product. We have increased the front reflectivity from 0.32 as described in the previous section, to 0.78, so that the number of quantum wells required in the active region could be reduced by a factor of ≈ 3 (from 70 to 24). It should be noted that although the optical bandwidth in terms of contrast ratio decreases in the present devices compared to the previous AFPs, at ≈ 2 nm it still remains about half that of the room temperature exciton linewidth (≈ 3.5 nm).

The structure shown in Figure III.5 was grown using molecular beam epitaxy. The bottom mirror was made of $20^1/_2$ periods of alternating 725 Å AlAs and 625 Å $Al_{0.2}Ga_{0.8}As$ layers doped with Si to ≈ 10^{18} cm^{-3} grown on an n^+-GaAs substrate. The active region has 24 pairs of undoped 100 Å GaAs/100 Å $Al_{0.2}Ga_{0.8}As$ MQW.

Figure III.6 shows a broad band spectrum of such a structure without bias. The reflectivity is relative to that of a gold mirror (R_{max} ≈ 98%). Measured FP mode positions agree quite well with a calculation in which the refractive index was taken from Ref. [17] and the MQW was modeled as $Al_{0.1}Ga_{0.9}As$, as discussed above. The modulation is applied to the center FP mode. The extra valleys in the spectrum are due to heavy hole and light hole excitons, as marked in Figure III.7.

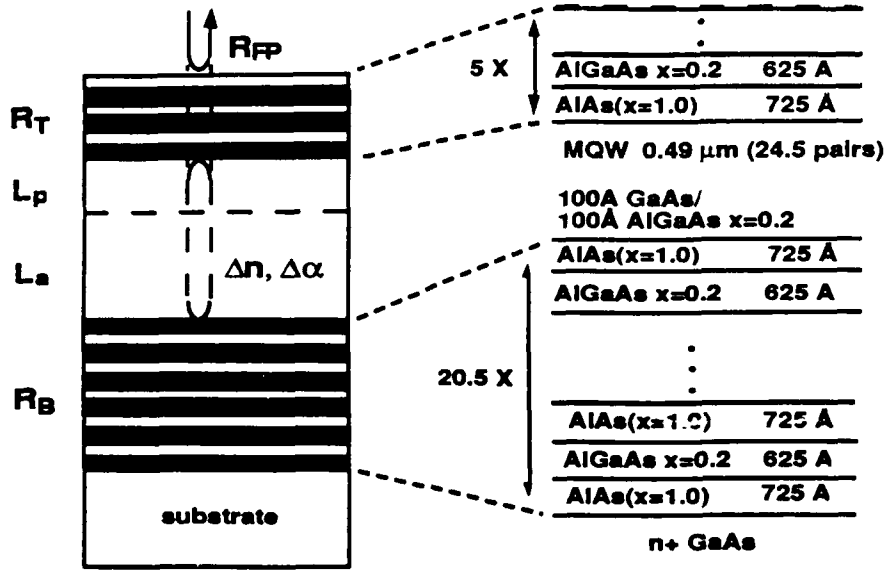

Figure III.5

Schematic of the epitaxial structure of the low-voltage AFPM with a ≈ 78 % top mirror reflectivity.

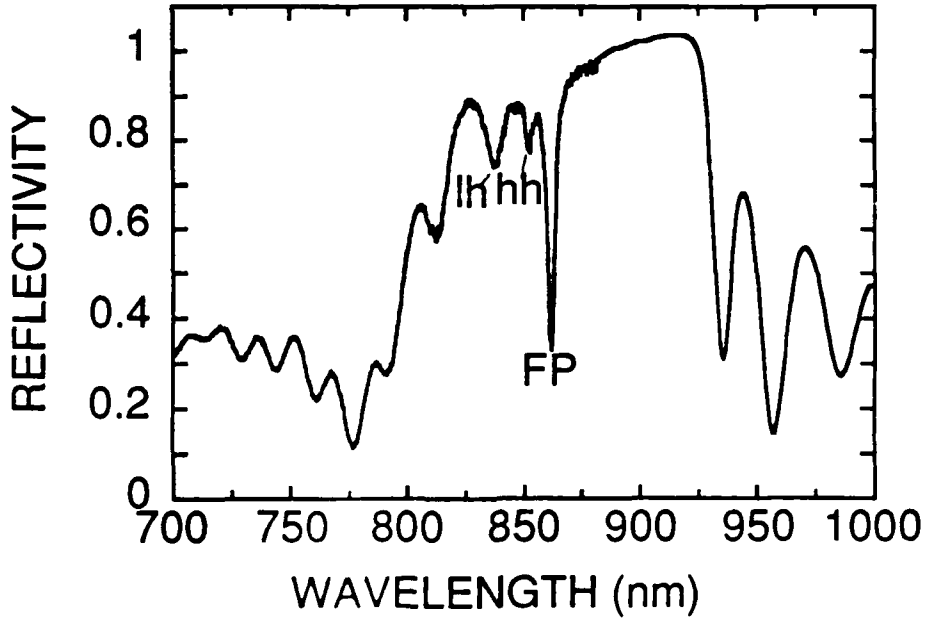

Figure III.6

Broad-band spectrum without bias for the structure shown in Figure III.5. The heavy hole (hh) and light hole (lh) exciton position as well as the Fabry-Perot mode (FP) are indicated.

Shown in Figure III.7 are the narrow band spectra for reverse bias voltages between 0 and -2.5 volts for the same device as in Figure III.6. The positions of excitons and Fabry-Perot modes are indicated. The exciton moves from 854 to 861 and 865 nm, as the field increases from 30 (built-in field) to 70 and 90 kV/cm, respectively. Small shifts of the FP mode are also observable.

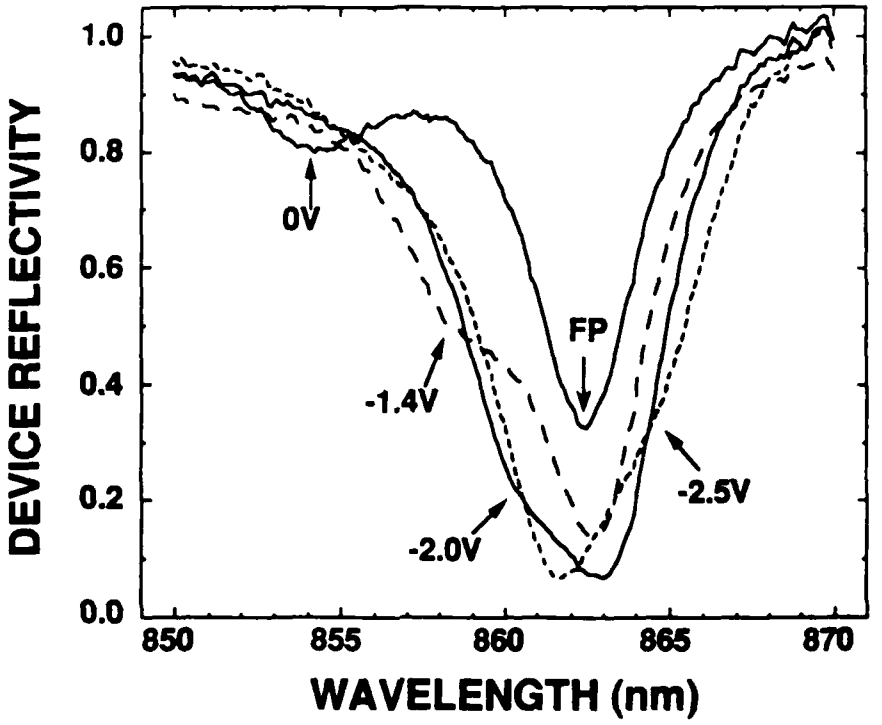

Figure III.7

Narrow band spectra for reverse bias voltages of 0, -1.4, -2.0 and -2.5 volts for the AFPM structure in Figure III.5.

Figure III.8 shows the reflectivity as a function of voltage signal at the wavelength of 864.3 nm for another device on the same wafer. A highly non-linear reflection response as a function of applied voltage is observed, as is typically found in FP-type modulators. The contrast ratio in this case is more than 50 and the reflectivity changes more than 40 % when the voltage varies from -1 to -3 volts. Varying the operating wavelength, we have observed essentially the same amount of reflectivity modulation, but the contrast ratio degrades to be below 10 dB as the wavelength moves (more than ≈ 1 nm) away from 864.3 nm. Therefore, the AFPM is suitable for high-contrast mode of operation if the light source wavelength can be well controlled. On the other hand, high M_v tends not to be so sensitive to the wavelength variations.

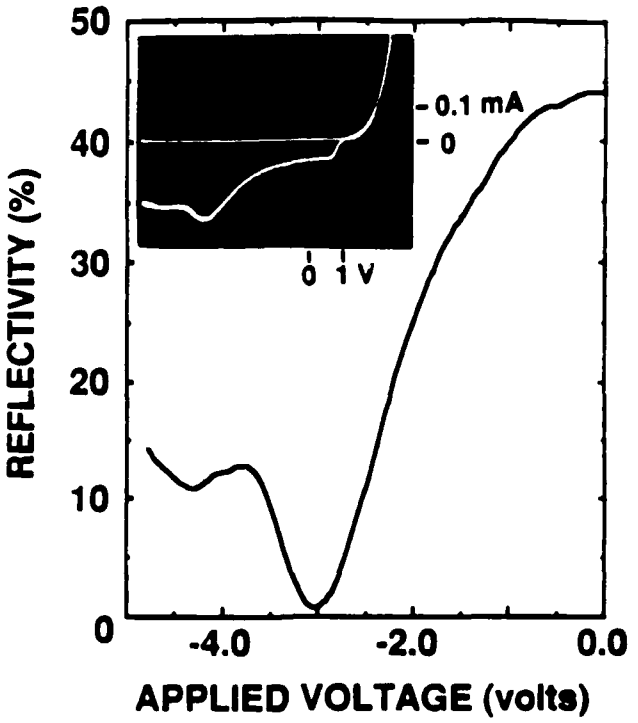

Figure III.8

Reflectivity versus applied voltage at 864 nm for the device shown in Figure III.7. The inset is the photocurrent trace.

By defining a modulation transfer function (M_v) as the percentage reflection change per unit operating voltage swing, more than 20 %/V is achieved in our structures. That is, one needs to apply only 1 volt to change the optical power by a quarter. Or, for sinusoidal modulation in a 50 Ω drive system, full modulation depth requires only 10 mW of drive power. Such a device is very suitable to be driven by modern high speed transistors which are usually operate with voltages of ≈ 1-2 volts.

Since the AFP is operated with the electro-absorption effect of MQW's, a strong photocurrent signal is detected for all bias conditions. Note that the built-in voltage of ≈1.5 volts gives a field of ≈ 30 kV/cm which is sufficient to provide the bias for detection. Shown in the inset of Figure III.8 is a photocurrent measurement as a function of bias voltage also at 864.3 nm. The detector response is voltage-dependent, as expected. Since the transmission through the AFP is quite small (≤ 3 %), the fraction of the light that is absorbed in the active region (A) is approximately equal to one minus the reflected power relative to the input power (R), i.e. A ≈ 1-R. So if the input optical signal carries a bit stream, the modulator can be used as a detector. Such a function has recently been demonstrated [1], and the results would be improved further with the low-voltage AFP modulators.

III.4. Optimization of the AFPM

As far as device design is concerned, R_T is one of the most important parameters to vary for a given material with known electro-absorption characteristics. As R_T increases, the $\alpha \cdot l$ product required to change from on to off or vice versa is decreased. For a given absorption change, the required cavity length, l, decreases, and the applied voltage V decreases since $V \approx F \cdot l$. However, the maximum reflection decreases and the range of $\alpha \cdot l$ for which gives very low reflectivity also decreases. The former effect indicates an increased insertion loss and the latter effect means the device performance is more sensitive to design and fabrication errors.

Another factor responsible for the insertion loss is the amount of "residual" absorption when the material is at minimum loss. With the QCSE, by choosing the FP mode wavelength, λ_{FP} closer to zero-field exciton wavelength, $\lambda_{ex(0)}$, smaller fields are required to shift the exciton to the FP mode and also larger absorption can be obtained. From Eq.(5) we know that the absorber thickness, l, can be made small. However, due to the finite linewidth of the exciton, the residual loss would be quite high, and therefore also the insertion loss. Furthermore, the sensitivity increases as the top mirror reflectivity increases. Conversely, by choosing λ_{FP} away from $\lambda_{ex(0)}$, lower residual loss can be obtained to decrease the insertion loss. However, the required field and absorber thickness increase, so the required voltage increases.

Using the excitonic electro-absorption model of Ref. [18], we have simulated the required voltage to achieve $\leq$ 3dB insertion loss, as a function of R_T, for AFP modulators. This is given by the solid line of Figure III.9. Note that the voltage here is defined as the product of the field and the required cavity length, F•l. In PIN diodes, built-in voltages on the order of 1.5 volts are present, and can serve as a bias. As R_T increases, V decreases initially due to the decreases of required cavity length. But when R_T becomes too large, the insertion loss becomes very sensitive to residual loss, and one needs to locate λ_{FP} further away from the zero-field exciton absorption edge to decrease the residual loss. As a result, larger fields, as shown by the dashed line of Figure III.9, as well as longer cavity length need to be used, and the required voltage swing increases again until the insertion can no longer be limited to 3 dB. The minimum voltage happens near $R_T \approx 0.76$ which is the design used in Section III.3.

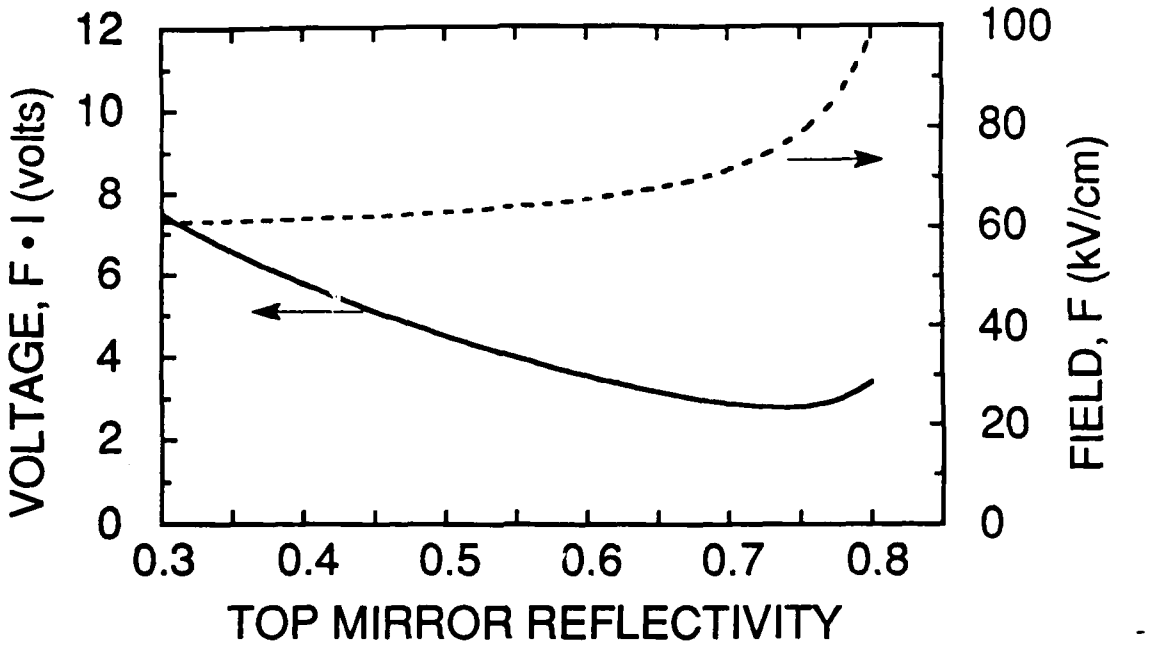

Figure III.9

The required voltage swing for the AFPM as a function of top mirror reflectivity (solid line). The required field is also shown in dashed line.

III.5 Comparison of Various Fabry-Perot Modulators

In asymmetric Fabry-Perot structures, R_T is made smaller than R_B. One could also design a structure with $R_T \approx R_B$, and use the the loss induced in the cavity to effectively decouple the bottom mirror reflectivity. In the limit as the induced loss increased, the net cavity reflectivity would tend towards R_T. The design of the mirrors would be similar to the index-tuned Fabry-Perot (SFPΔn) modulator, in that the reflectivities would need to be high to minimize insertion loss, and the cavity would be slightly asymmetric to compensate for residual loss in the absorber. We refer to this absorption-tuned quasi-symmetric Fabry-Perot as SFP$\Delta\alpha$.

To compare index- and absorption -tuned Fabry-Perot modulators, based on our previous measurements, we make the reasonable assumption that the MQW material has a maximum absorption change, $\Delta\alpha = 4000$ cm^{-1} and a maximum real refractive index change, $\Delta n = 0.3$ %.

Note that $(4\pi/\lambda)(\Delta n/\Delta\alpha) = 0.4$. This being less than 1 indicates that MQW material is more efficient in electro-absorption mode than in electro-refraction mode. All devices are modeled to have 3 dB insertion loss at their on-state, and zero-reflection at the off-state.

Figure III.10 plots the required cavity length to achieve the modulation between the on (50 %) and off (0 %) states as a function of the top mirror reflectivity. The advantage of the AFP is now obvious. SFP$\Delta\alpha$ and SFPΔn-type devices are found to be comparable in term of the required cavity length. Data points shown in Figure III.10 illustrate the agreement of our experiments with the simple model.

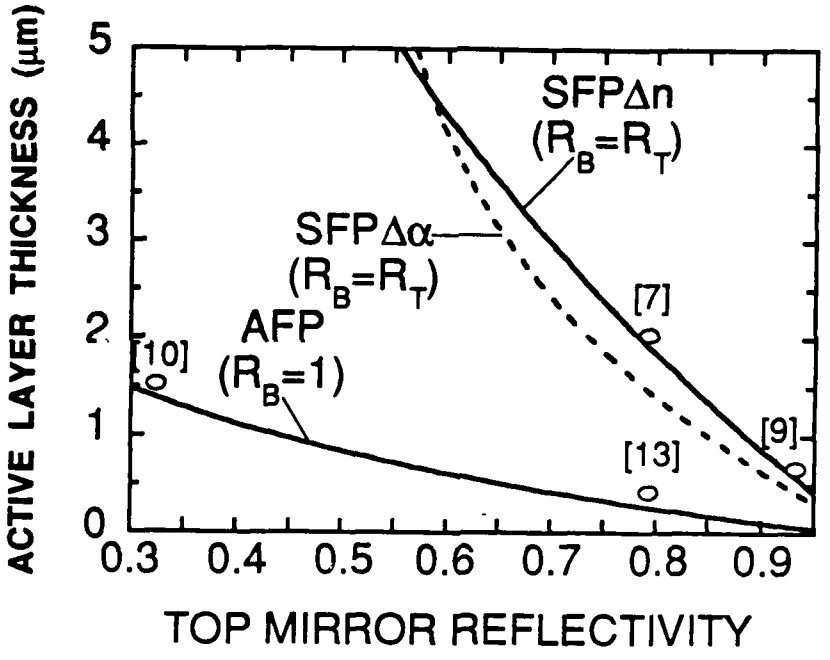

Figure III.10

A comparison of the required cavity length for various Fabry-Perot modulators. Actual device designs are also indicated from the cited references.

It should be noted that for the same R_T, smaller required cavity lengths represent wider optical bandwidth BW_o because optical bandwidths are inversely proportional to the product of the *finesse* and the effective cavity length, which is the sum of the actual cavity length and the grating mirror penetration length. More detailed discussions on optical bandwidths are given in Section III.6.

III.6. Sensitivity Analysis

Resonator-type devices are known to be sensitive to operating conditions. Although the AFP modulators mentioned above usually have low *finesse* (≤ 10), variations in wavelength, voltage, temperature, and thickness uniformity will have some bearing on the stablility of the device operation. We analyse these effects in this section.

In general, the AFP requires the right amount of absorption (α_{op}) induced at the right wavelength (λ_{FP}), near which wavelength (λ_{op}) the optical signal is operating. The absorption at λ_{FP} is determined by the applied field (F) and the relative wavelength shift between λ_{FP} and $\lambda_{ex(0)}$, the zero-field exciton position. Our design is to use F_{op} to shift the exciton from $\lambda_{ex(0)}$ to λ_{FP} to induce the required absorption α_{op} to turn off the AFP as given by eq.(5):

i.e. $\alpha_{op} = (2l)^{-1} \ln (R_B/R_T)$.

A variation in F and $\lambda_{ex(0)}$ would cause the induced absorption, α, to be different from α_{op}, making the off-level non-zero. The on-level would of course be changed due to these variations, but it is less sensitive than the off-level, because the latter is the one that determines the contrast ratio the most. Therefore, the sensitivity is determined by the variation of the off-level to the variations in wavelength and absorption. Variations in F are due to variations in applied voltages, while variations in $\lambda_{ex(0)}$ could be due to thermal drift of the bandgap energy and/or non-uniformity in the layers.

III.6a. Operating Wavelength Variations - Optical Bandwidth

When reflection modulators are in their off-state, the reflection stays low only over a certain wavelength range, as shown schematically in the inset of Figure III.11(a). Assuming the on-state is 50 % reflective and the system requires 10 dB contrast, the optical bandwidth is the wavelength range over which R_{off} (off-state reflectivity) stays below 5 %. Following the procedure in Ref. [9], we have the following expression for the allowable wavelength variation $\Delta\lambda_{op}$ with respect to λ_{FP}:

$$\Delta\lambda_{op} = \pm \frac{\lambda_{FP}^2}{4\pi n\left(1 - \frac{\lambda}{n}\frac{dn}{d\lambda}\right)(1 + L_{eff,T} + L_{eff,B})} \cos^{-1}\left[1 - \frac{\left(\frac{1 - R_T}{2 R_T}\right)^2 R_{off}}{1 - R_{off}}\right] \qquad (6)$$

where λ_{FP} is the Fabry-Perot mode wavelength, l is the active region thickness, $L_{eff,T(B)}$ is the penetration depth in the top (bottom) grating, and R_{off} is the requirement on the reflection in the off-state which is set at 5 % in our example. For convenience, we assume $L_{eff,T}+L_{eff,B}$= 1 μm, although the actual values depend on the design of the grating mirrors.

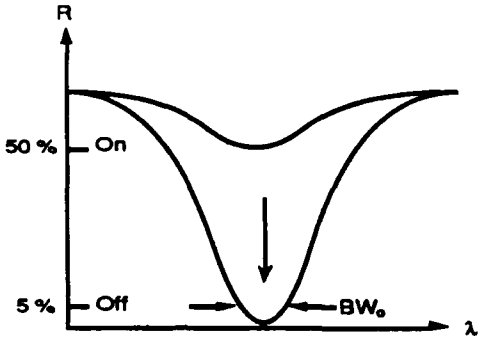

(a)

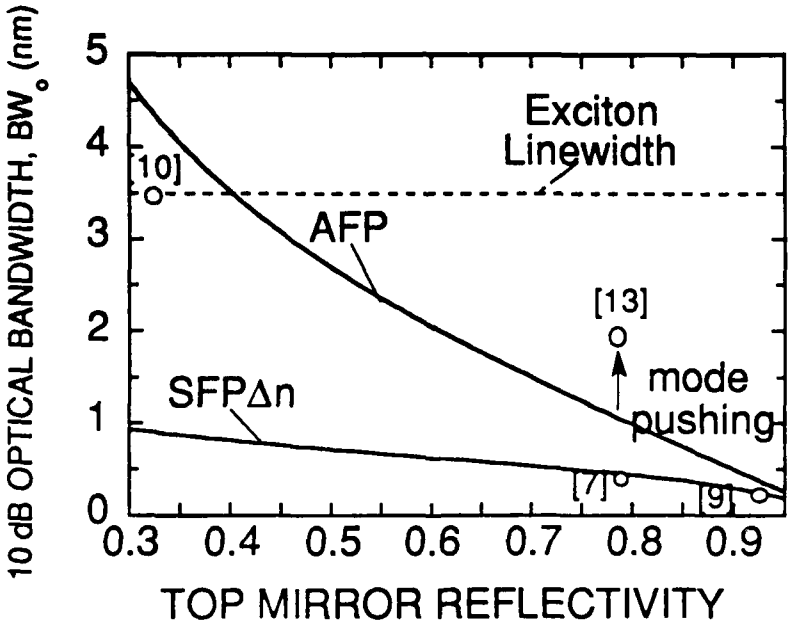

(b)

Figure III.11

(a) Schematic drawing for defining optical bandwidth. (b) Calculated optical bandwidth for SFPΔn and AFP as a function of top mirror reflectivity. Data points are also included from the indicated references.

Figure III.11(b) plots the 10 dB optical bandwidth BW_o, given by $2 \cdot |\Delta\lambda_{op}|$ based on the active region thickness requirement calculated in Figure III.10 (Section III.5). The measured optical

bandwidths of various devices are also indicated. Reasonable agreements have been obtained, and therefore the optical bandwidth of Fabry-Perot type devices is mainly determined by the structure itself, rather than the material's electro-optical effect, because the optical bandwidth is somewhat smaller than the exciton linewidth. The one exception is the AFPM with R_T=0.32. Because the *finesse* is only ≈ 2, this device has a material-limited optical bandwidth.

III.6b Voltage Swing Variations

Variations in voltage, i.e. variations in field, would cause the absorption in the MQWs at the FP mode to deviate from design values. The analysis shown in Figure III.12 models the effect of variation of absorption on the off-level due to variations in field (F) and zero-field exciton position ($\lambda_{ex(0)}$). Wavelength variation can also be interpreted as variation in the operating wavelength or the position of the Fabry-Perot mode. So the variation in wavelength can be discussed in terms of the difference of the operating wavelength (FP mode) and the zero-field exciton position, $\Delta\lambda \equiv \lambda_{FP}-\lambda_{ex(0)}$.

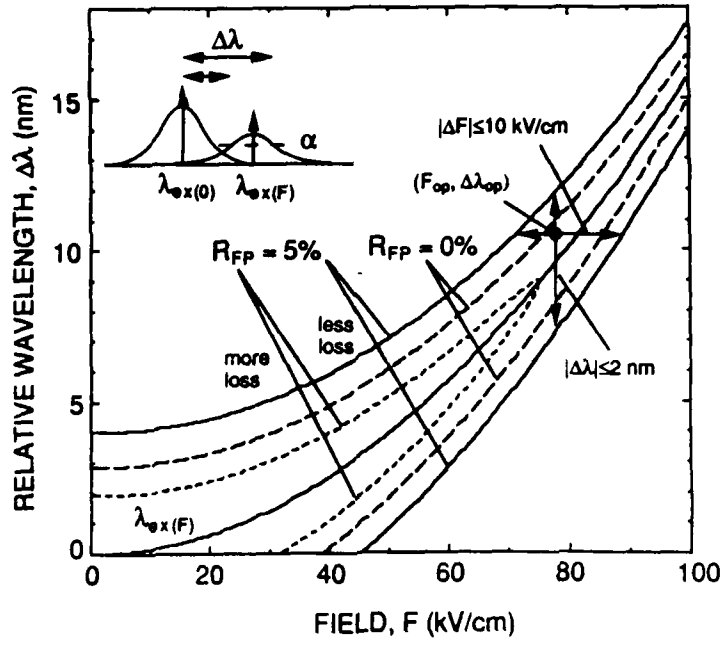

Figure III.12

Sensitivity of the applied field and the zero-biased exciton position. See the text for discussion.

The inset of Figure III.12 schematically shows the heavy-hole excitonic absorption as a function of wavelength under applied electric field. For a given Fabry-Perot cavity loss value, α, one can trace the contours of field and wavelength shift (F, Δλ) to give the same value α.

Due to the Lorentzian shape of the excitonic line, there may be more than one branch of such curves. In other words, under a given field there may be more than one wavelength shift ($\Delta\lambda$) that gives α, as illustrated in the inset.

Figure III.12 shows the absorption contours corresponding to R_{off}=0 and 5 % for the 2 V AFP modulator described in Section III.3. The dashed lines represent the contours for R_{off}=0% (absorption=2271 cm^{-1}). Due to the Lorentzian line shapes as mentioned, there are two branches for R_{off}=0 %. For R_{off}=5 % there are two absorption values, 1324 (less loss) and 3770 (more loss) cm^{-1}, shown in solid and dotted lines, respectively, as indicated. There are four branches for R_{off}=5 %. There are two zones defined by the two different absorption contours, within which zones R_{off} stays below 5 %. The two zones merge where the higher loss contours stop, since the higher loss value is actually larger than the peak absorption of the exciton. This condition is satisfied when the loss contour meets the exciton peak position trace (also in solid line) as a function of field.

Our design is to locate the operating condition near the point where the two zones merge to give the most tolerable operating variations. As one can see, the merged zone gets narrower as the field or the wavelength shift increase. The experimental operating point is indicated by the dot (F_{op}, $\Delta\lambda_{op}$). It should be noted that the lower zone corresponding to the short wavelength side of the heavy-hole exciton only represents partial information. The actual situation may be more complicated due to the presence of the light-hole exciton and the onset of the continuum transitions. To maintain low insertion loss, λ_{FP}-$\lambda_{ex(0)}$ should be kept above some value due to the finite linewidth of the hh-exciton. For example, λ_{FP}-$\lambda_{ex(0)}$ needs to be >10 nm for maintaining less than 3 dB insertion loss, although at this point we have experimentally observed ≈ 4dB insertion loss.

When the applied field is F_{op}, the tolerance in the wavelength shift is ≈ ± 2 nm, as represented by a segment of vertical line in Figure III.12 passing through the operating point to maintain $R_{off} \leq 5\%$. Note that this is the tolerance in λ_{FP}-$\lambda_{ex(0)}$, not in the operating wavelength. The actual tolerance in the operating wavelength is more determined by the FP mode linewidth (± 1nm), as described in III.6a). Similarly, with the right wavelength shift, $\Delta\lambda_{op}$, the tolerance in field variations is ≈ ±10 kV/cm as indicated by a horizontal line segment. For a 0.5 μm thick active region, the tolerable voltage variation is ≈ 0.5 volts, which agrees with experimentally determined values as in Figure III.8. This 20 % voltage tolerance represents the sensitivity of the AFP of *finesse* 12 to applied voltage variations.

III.6c. Non-uniformity and Thickness Variations

Variation in thickness and composition would cause variation in Fabry-Perot mode position and zero-field exciton wavelength. Assuming only the layer thickness is varied, the Fabry-Perot mode is much more sensitive than the exciton position for the particular MQW structure that we use (100Å wells). Therefore the discussion can be focused on the effect of the Fabry-Perot mode variations.

First of all, variation in the position of the FP mode would cause misalignment between the FP mode and the operating wavelength, similar to section III.6a. Thus, the tolerable FP mode variation ($\Delta\lambda_{FP}$) is again given by Figure III.11(b): i.e.$|\Delta\lambda_{FP}| \leq 1$nm, or $|\Delta\lambda_{FP}/\lambda_{FP}| \leq 0.12\%$. This is probably the most severe constraint on AFPMs. If the operating wavelength can track the FP mode, then the variation in FP mode causes the variation in λ_{FP}-$\lambda_{ex(0)}$ as in Figure III.12. In this case the tolerance is determined from Figure III.12 to be $|\Delta\lambda_{FP}| \leq 2$nm.

III.6d. Temperature Variation

Variation in temperature causes a drift of the bandgap energy and a change of the refractive index. The former changes the exciton position while the latter varies the FP wavelength. Figure III.13 shows the temperature-dependent zero bias reflection spectrum of the AFPM described in Section III.3. The two reflection dips correspond to the heavy hole exciton and FP mode, as indicated. As seen from Figure III.13, the heavy hole exciton shifts three time faster than the FP mode [19].

Figure III.14 shows the temperature-dependent modulation of the AFPM as a function of voltage. λ_{op} is chosen to be λ_{FP} (862 nm) at 20 °C. The transfer function is smaller (≈13 %/V) than the peak value of 23 %/V, which is observed at another wavelength. One sees immediately that as the temperature increases from 20 to 35 °C, the insertion loss initially increases due to the increased residual loss caused by the approaching of the exciton. After that, the insertion loss does not vary much because λ_{op} and λ_{FP} are no longer aligned. As the temperature increases, the separation between λ_{ex} and λ_{op} decreases, so one does not have to apply as large a field to shift the exciton to λ_{op}, and the required voltage to achieve minimum reflectivity decreases. Although the difference between high and low reflectivity decreases as the temperature increases, the transfer function remains about the same 13 %/V from 15 to 30 °C, and degrades a little at 35 °C. However, the contrast degrades a great deal.

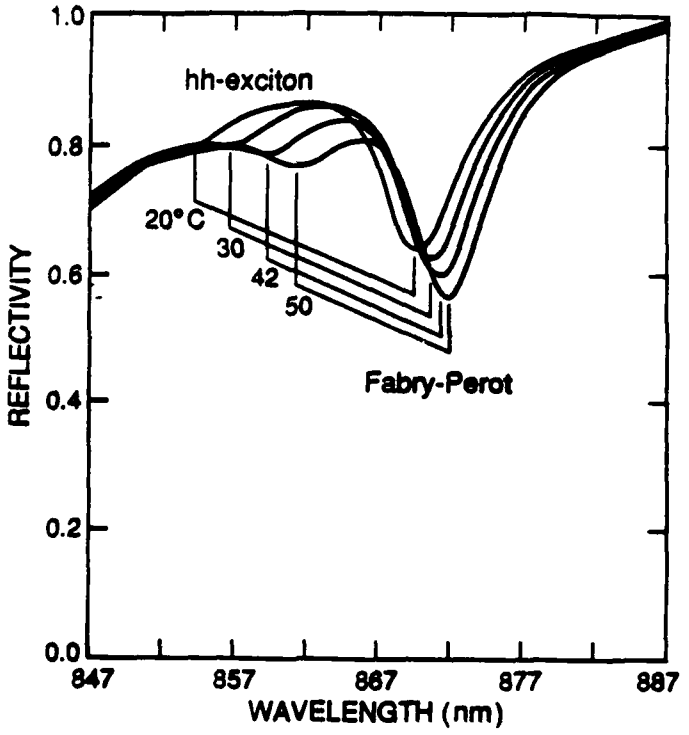

Figure III.13

Temperature-dependent zero bias reflection spectrum of the asymmetric Fabry-Perot structure of Figure III.5.

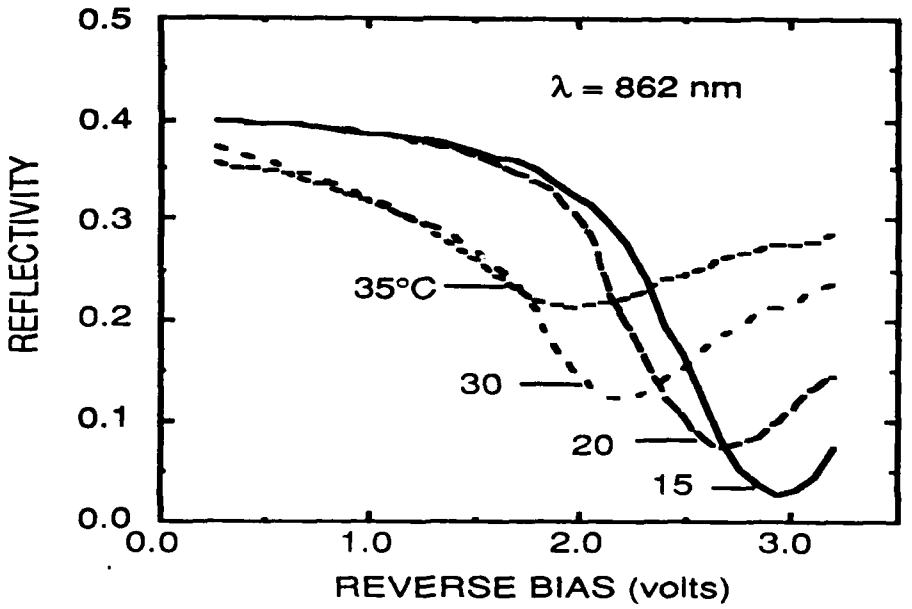

Figure III.14

Temperature dependent modulation as a function of applied voltage of the asymmetric Fabry-Perot modulator as in Figure III.7. The operating wavelength is 862 nm.

Similar to the discussions in Section III.6c, due to $\Delta\lambda_{FP}$, the operating wavelength λ_{op} is misaligned with λ_{FP} and the tolerable $\Delta\lambda_{FP}$ is $\approx \pm 1$ nm or ± 10 °C for AFPMs. In addition to $\Delta\lambda_{FP}$, the exciton is also shifted, and λ_{FP}-$\lambda_{ex(0)}$ shifts at a rate of 1.8 Å/°C. If the operating wavelength tracks the FP mode, from the requirement of $\Delta(\lambda_{FP}-\lambda_{ex(0)}) \approx \pm 2$nm, we know that the temperature tolerance is also $\approx \pm 10$ °C. If the operating wavelength is fixed, the tolerance in temperature would be less than 10 °C for high contrast. On the other hand, large reflectivity change can be obtained with much larger operating tolerances.

It is interesting to note that without the FP resonance, $\lambda_{ex(0)}$ determines the operating wavelength. For a fixed operating wavelength, the tolerance to temperature variations is smaller because $\frac{\partial\lambda_{ex}}{\partial T}$ is larger than $\frac{\partial\lambda_{FP}}{\partial T}$. On the other hand, if the operating wavelength tracks the exciton, the tolerance to temperature variations is much larger.

III.7 Superlattice AFPM with a Normally-Off Characteristic

Although all of the work on AFP modulators discussed in the previous sections has used the quantum confined Stark effect (QCSE) in QWs, we have also demonstrated a device which exploits the Field Induced Stark Localization effect in a superlattice (SL) [20], for which we described initial experimental results in our previous report. By "superlattice" we mean a structure where the wells and barriers are of a thickness such that the quantum-confined energy states are no longer sharply defined, but broadened into minibands in the absence of an electric field. In contrast to the absorption-edge red shift in QWs due to the QCSE, the SL absorption edge shifts to the blue with increasing field due to the localization of extended states in both conduction and valence minibands in the SL. Essentially the absorption edge sharpens up with bias. This phenomenon, generally referred to as Wannier-Stark localization [21], has been observed at room temperature [20] and potentially offers lower voltage operation than the QCSE.

Our SL-AFP [22] contains a SL (100 1/2 pairs of 30Å GaAs / 30Å $Al_{0.3}Ga_{0.7}As$) active layer in between a highly reflective bottom mirror, which is a quarter-wave ($\lambda/4$) stack (15 1/2 periods of alternating 618Å AlAs and 535Å $Al_{0.3}Ga_{0.7}As$ layers), and a less reflective top mirror, which is an air-semiconductor interface ($R \approx 0.3$). The off-level of the SL-AFP at

zero-bias is achieved by aligning the Fabry-Perot (FP) resonance at the appropriate wavelength relative to the low (or zero) field absorption edge with enough absorption so that the effective reflection from the bottom mirror viewed through the absorptive cavity cancels the reflection from the top. The on-level is attained by reducing the cavity loss using a field-induced blue shift of the SL absorption edge upon application of sufficient field.

Fig. III.15 shows the narrowband spectra of the SL-AFP device under different reverse biases. The reflectivity at the zero-bias Fabry-Perot mode increases with increasing bias and reaches a value of 25% at -8V.

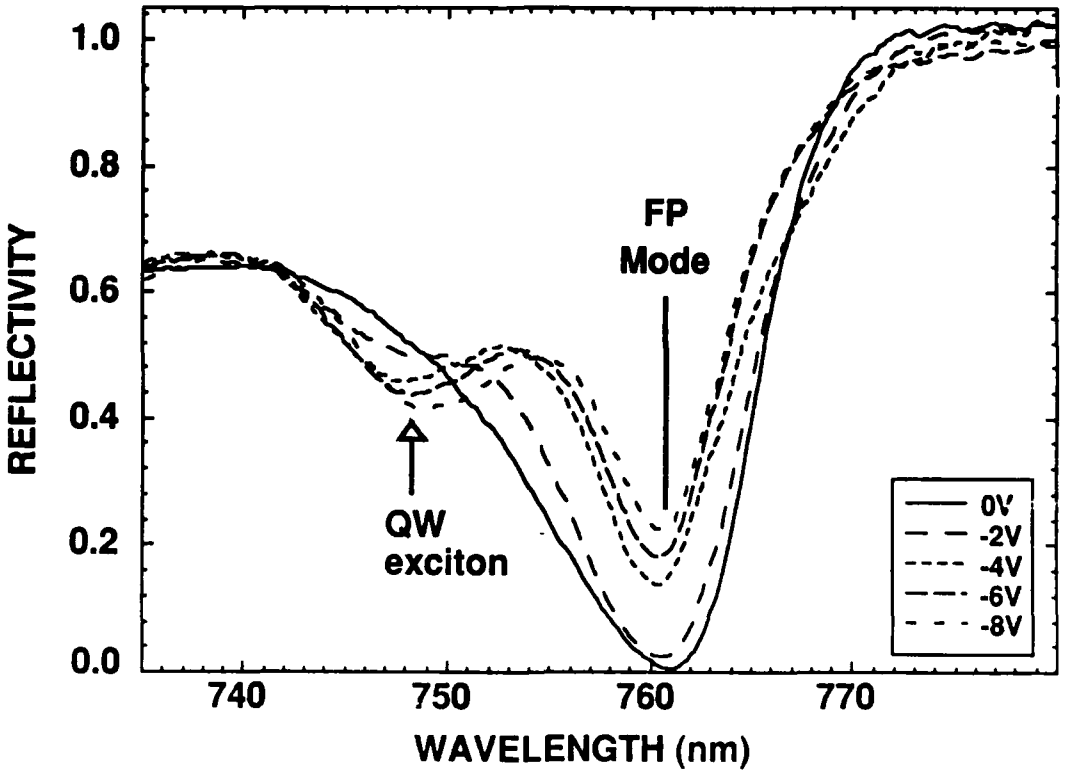

Figure III.15

Narrowband reflection spectra of the SL-AFP device under different reverse biases.

Fig. III.16 shows the photocurrent measurements of the SL-AFP as a function of wavelength at various reverse biases. The photocurrent (I_{ph}) spectra are voltage dependent as are the reflectivity counterparts. In this device, the fraction of light that is absorbed inside the cavity's active material is approximately equal to one minus its resultant reflectivity since the transmission through the SL-AFP is only a few percent. At the zero-bias resonant wavelength

(≈ 7620Å), the net reflectivity R_{FP} of the SL-AFP is essentially zero when there is sufficient but not excessive loss inside the cavity. Therefore the incident light is totally absorbed and the I_{ph} is at its maximum at resonance. As the applied electric field is increased beyond the built-in value, R_{FP} is turned on by reducing the cavity loss at resonance through the blue-shifted electroabsorption effect of Wannier-Stark localization in the superlattice. The I_{ph} around the resonance wavelength decreases with increasing field as a result. There is a progressive emergence of a peak at ≈ 7460Å with increasing field which is due to the recovery of the QW exciton as a result of Wannier-Stark localization. Fig. III.16 shows that negative differential resistance is observable over a wide range of wavelengths (≈ 7500Å to 7650Å). The existence of this negative differential resistance is a necessary condition for successful demonstration of a Self Electro-optic Effect Device (SEED) [23].

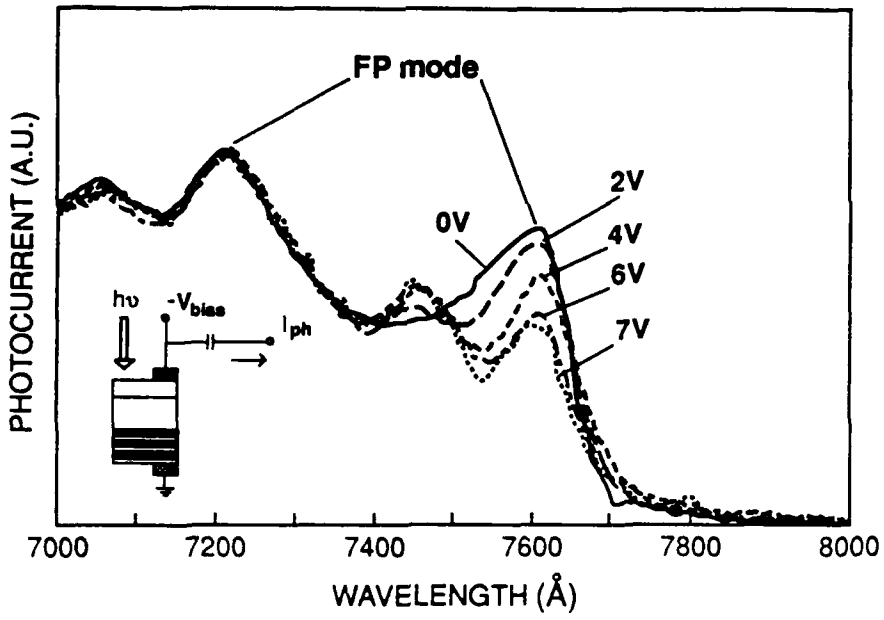

Figure III.16

Photocurrent spectra of the SL-AFP at different reverse biases. The structure exhibits negative differential resistance over a wide range of wavelengths (~7500Å to 7650Å). The inset shows the experimental schematic for the photocurrent measurement where conventional lock-in technique was used.

III.8 Superlattice AFP Self-Electro-Optic-Effect Device (SEED)

There has been considerable interest in optical switching devices using both semiconductor quantum wells (QWs) and superlattices (SLs). SEEDs are one class of such devices, and are promising elements for future optical information processing systems. The term "SEED" generally applies to any combination of modulator and photodetector which allows the optical output of the device to be set by an optical input. In a quantum well SEED (QW-SEED), a MQW modulator is usually connected in series with a reverse-bias voltage supply and a load element such as a simple resistor. By increasing the incident light intensity at an operating wavelength which coincides with the zero-field QW exciton peak, switching and optical bistability due to positive feedback can be obtained [23]. Also, a more sophisticated load such as a photodiode (or another similar modulator) can be connected in series to form a diode SEED (D-SEED) [24], or a symmetric SEED (S-SEED) [25] to achieve better bistability loop characteristics.

We have exploited the potential of the SL-AFP as a very high-contrast normally-off modulator by connecting the SL-AFP in series with a photodiode and a reverse-biased voltage supply to form a high performance superlattice Fabry-Perot self-electro-optic effect device (SL-FP-SEED) [26].

The SL-FP-SEED configuration is shown in Fig. III.17(a) where the SL-AFP is connected in series with a Si photodiode and a reverse bias voltage supply ($\approx$ 7.5 volts). When both the control beam (power P_{in1}) and signal beam (power P_{in2}) are incident upon the Si photodiode and the SL-AFP respectively, they give rise to photocurrents in the circuit. The current through the Si photodetector must be equal to that through the SL-AFP at steady state, and the voltage across it adjusts itself to ensure this condition is satisfied. The reflected optical output (power P_{out2}) from the SL-AFP is modulated as the voltage across it changes. The operation of this device can be readily understood by considering the photodetector as load for the SL-AFP, as shown in Fig. III.17(b). Here the Si photodetector input intensity is varied and that to the SL-AFP modulator is fixed. The device is bistable whenever there are three intersection points [23], and this will be the case if the SL-AFP is operated at a wavelength where absorption decreases with increasing voltage. Like the S-SEED [25] this device will only be bistable when the optical input power levels are comparable (line B), and only one single state will exist if the incident power onto the SL-AFP is much higher than that onto the Si photodiode and vice versa (lines A and C respectively).

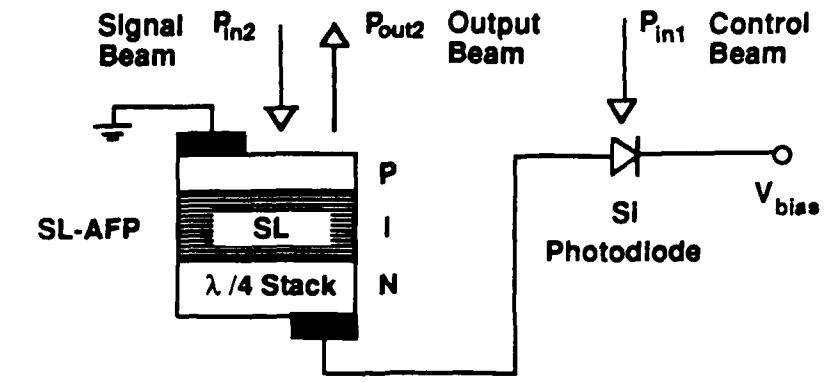

(a)

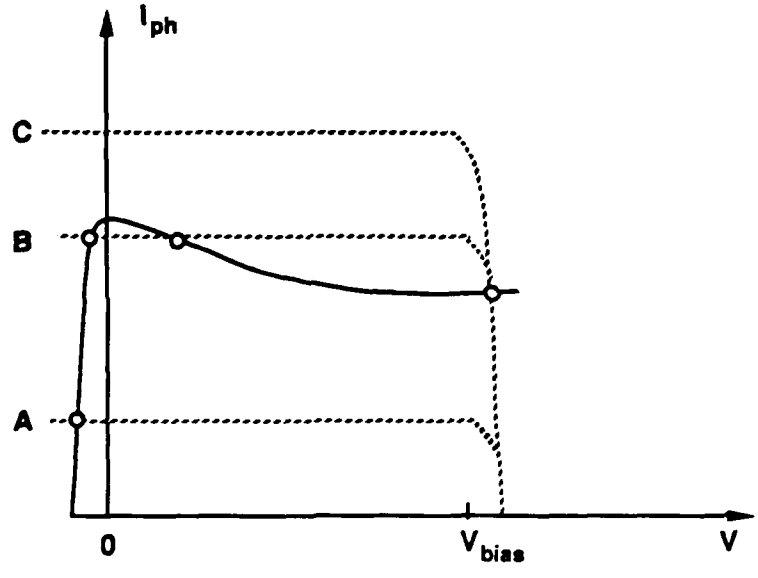

(b)

Figure III.17

(a) Schematic set-up of the SL-AFP-SEED. P_{in1} and P_{in2} are the incident light power of the Si photodiode and the SL-AFP, respectively. P_{out2} is the reflected output power from the SL-AFP that can be switched by varying P_{in1}.

(b) Load lines of both the SL-AFP and the Si photodiode. Solid curve is the photocurrent vs voltage for the SL-AFP at one particular input intensity P_{in2}. Dashed lines are the photocurrent vs voltage for the Si photodiode at three different input intensities P_{in1}. Line B shows that the device is bistable because there are three intersection points between the SL-AFP and the Si photodiode load lines.

Fig. III.18 shows the reflected power from the SL-AFP as a function of applied voltage at a wavelength ≈ 7620Å. The reflected power reached the zero line when the incident light onto the SL-AFP was blocked. A high contrast ratio of >100:1 has been obtained at this wavelength.

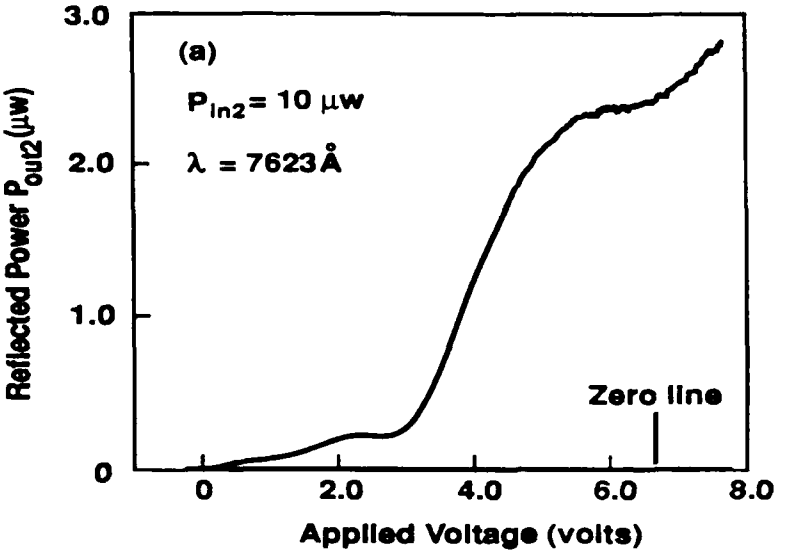

Figure III.18

Reflected power of the SL-AFP as a function of voltage at the wavelength 7623Å. The reflected power reached the zero line when the optical input beam onto the SL-AFP was blocked.

With the SL-AFP in the SL-FP-SEED configuration (Fig. III.17(a)), we tested for optical bistability by shining light onto the Si photodiode using a commercial GaAs laser diode and illuminating the SL-AFP with the Ti:sapphire laser. The output power of the Ti:sapphire laser was set to be constant for each measurement. The GaAs laser power was ramped up and down to cause the SL-AFP 's output to switch state.

Fig. III.19 shows the reflected optical power (P_{out2}) from the SL-AFP as a function of incident intensity (P_{in1}) onto the photodiode for two different signal beam powers (P_{in2}). Optical

bistability in the SL-AFP 's reflected power with respect to the photodiode's input power could clearly be seen. As shown in Fig. III.19, an on/off ratio of about 130:1 in the reflected power output was also attained. The output of the device also scaled linearly with the P_{in2}. Likewise, the device's bistability loop width also varied proportionally with P_{in2}, as expected [23]. Optical bistabilty could be observed in a wide spectral range and an on/off ratio of more than 10:1 was obtained over an optical bandwidth of ≈ 30Å.

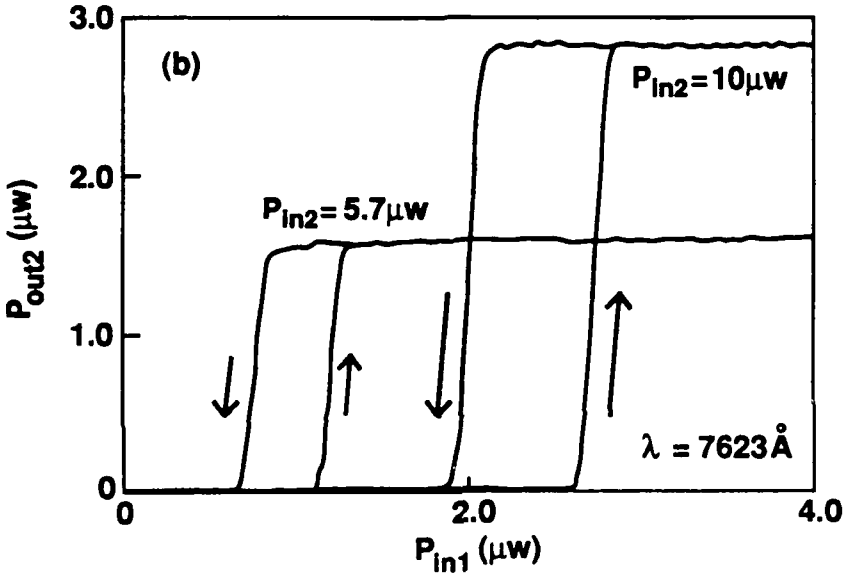

Figure III.19

Output power (P_{out2}) reflected from the SL-FP-SEED vs control power (P_{in1}) for different signal powers (P_{in2}). An on/off ratio in P_{out2} of ≈130:1 was attained.

The potential advantage of incorporating SL-AFP into SEEDs can be further extended by connecting two such modulators in series with a reverse-bias voltage supply to form a high performance S-SEED. The external bias voltage of such an S-SEED can also be reduced or eliminated by employing SL-AFPs with lower operating voltage, obtained by properly reducing the active region thickness and increasing the top mirror reflectivity.

IV. High-Frequency Operation of Fabry-Perot Modulators

The modulation measurements we have discussed in this report (and in previous ones) have all been taken at relatively low frequencies, our intent being of course to demonstrate and compare the capabilities of various device structures while keeping post-growth device processing to a minimum. Modulation speed is, nevertheless, extremely important for most of the information processing and optical interconnection applications whose promise sparked our interest in Fabry-Perot modulators in the first place. Since our last report, we have demonstrated 6.5 GHz small-signal modulation in a symmetric FP structure, and we are currently working towards the fabrication of devices which should run at 30 to 50 GHz.

IV.1. Device Structure and Fabrication

Our original Fabry-Perot modulator fabrication process consisted simply of evaporating p-contacts onto the MBE-grown material and then cleaving the wafer into reasonably small pieces for testing. Growing the FP étalons on N+ GaAs substrates enabled us to contact the n-doped mirror through the substrate, but the resulting devices were relatively large and slow.

In order to achieve higher-frequency modulation, we incorporated a highly-doped n-contact layer into the FP cavity to eliminate the series resistance through the substrate and back mirror, developed a two-level mesa fabrication process to delineate smaller, lower capacitance devices, and integrated these smaller devices with 50Ω coplanar microwave probe pads. To further reduce the series resistance, we graded the heterojunctions in the p-mirror. Figure IV-1 shows both cross-sectional and top views of a high-speed symmetric FP modulator identical to the one discussed in section II, except for the modifications just mentioned.

The high-speed fabrication process we chose to implement first (because of its relative simplicity) consists entirely of "wet" processes and is limited to devices no smaller than about 40μm on a side. The devices we fabricated have dimensions 40μm x 40μm, 60μm x 60μm, and 100μm x 100μm.

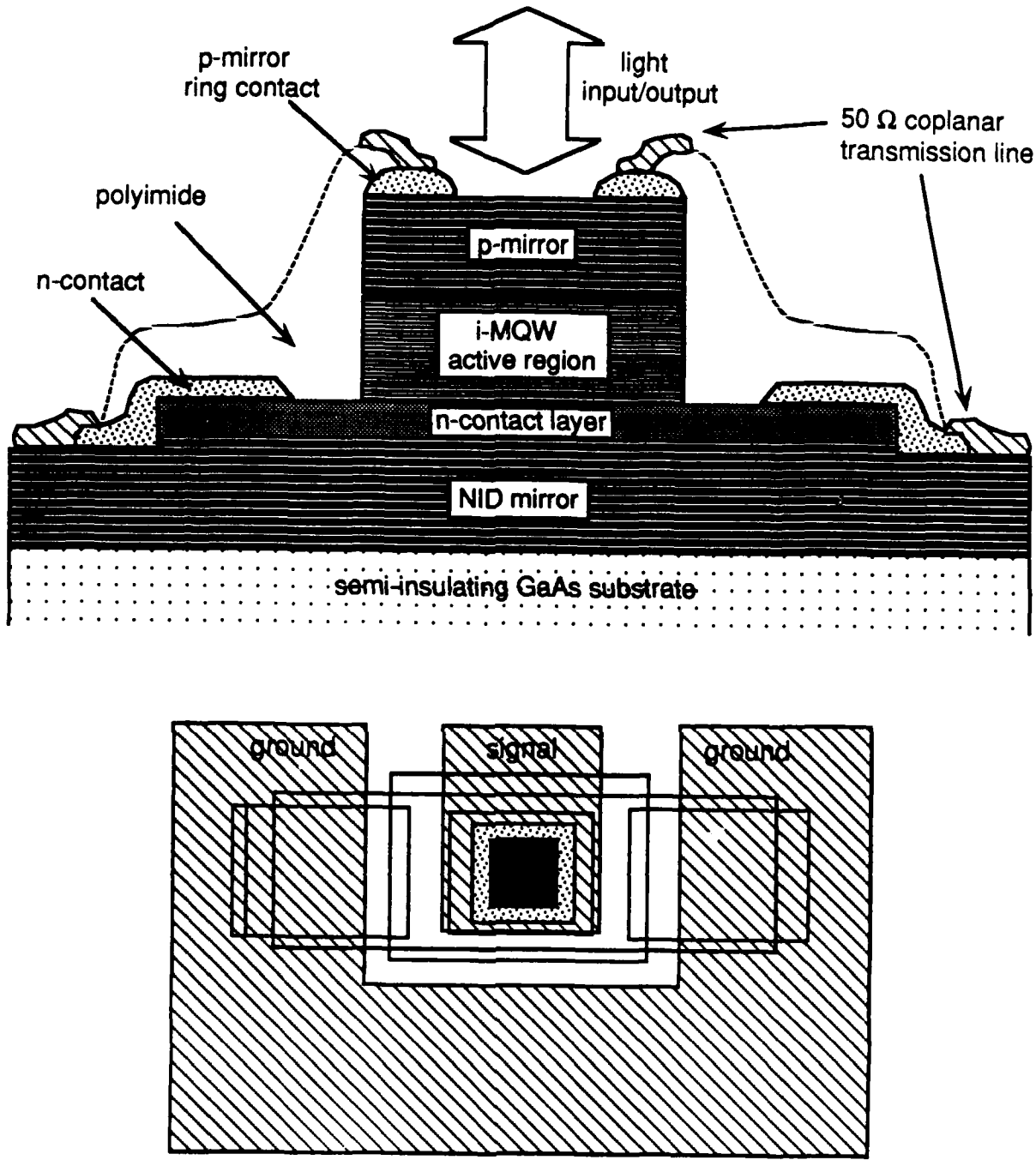

Figure IV-1

Cross-sectional and top views of a high-speed symmetric Fabry-Perot modulator.

IV.2. Electrical Characterization

Before optically testing our high-frequency modulators, we characterized them electrically both at DC and at microwave frequencies (using a network analyzer). First, we measured the sheet resistance of the n-contact and p-mirror layers as well as their respective contact resistances using TLM patterns on our mask. We also measured the capacitance of the three sizes of diodes. With these values we estimated the capacitance and series resistance of the devices. Then, using short and open calibration standards also included in our mask, we determined the equivalent circuit of the coplanar probe pads as shown in Figure IV-2, and measured the S_{11} of each device with the network analyzer.

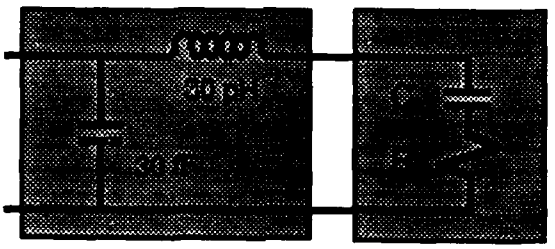

Figure IV-2

Equivalent circuit for a high-frequency modulator.

The resistance and capacitance values we extracted from these measurements agreed quite well with the values we calculated from our DC measurements. The table below details the measured resistance and capacitance of the modulators, the values of $f_\tau = 1/RC$ corresponding to the measured values of R and C, and, for easy comparison, the 3dB frequencies we determined from our small-signal optical measurements (discussed in section IV-3).

nominal diode size	electrical measurements			electrical 3dB frequency (GHz)	
	R (Ω)	C (pF)	at freq. (GHz)	predicted	measured
40μm x 40μm	36	0.28	5.0	6.6	6.5
60μm x 60μm	20	0.62	4.0	3.3	3.3
100μm x 100μm	14	1.71	1.2	1.5	1.0

IV.3. Small-Signal Modulation Results

With our estimated 3dB frequencies in hand, we set out to measure the small-signal modulation of our devices, using the apparatus pictured in Figure IV-3 (an extension of the dye laser set-up described in our last report). The measured modulation efficiency as a function of frequency for the three sizes of diodes is shown in Figure IV-4. The calculated performance given is simply the RC-limited response of the diodes. The fact that the theoretical and experimental curves agree so well implies that the speed of the devices is in fact limited by their resistance and capacitance, and not by material considerations such as carrier trapping in the quantum wells. We attribute the ripple which appears at about 2 GHz to uncalibrated reflections from the interface between the coaxial cables and the coplanar waveguide microwave probe.

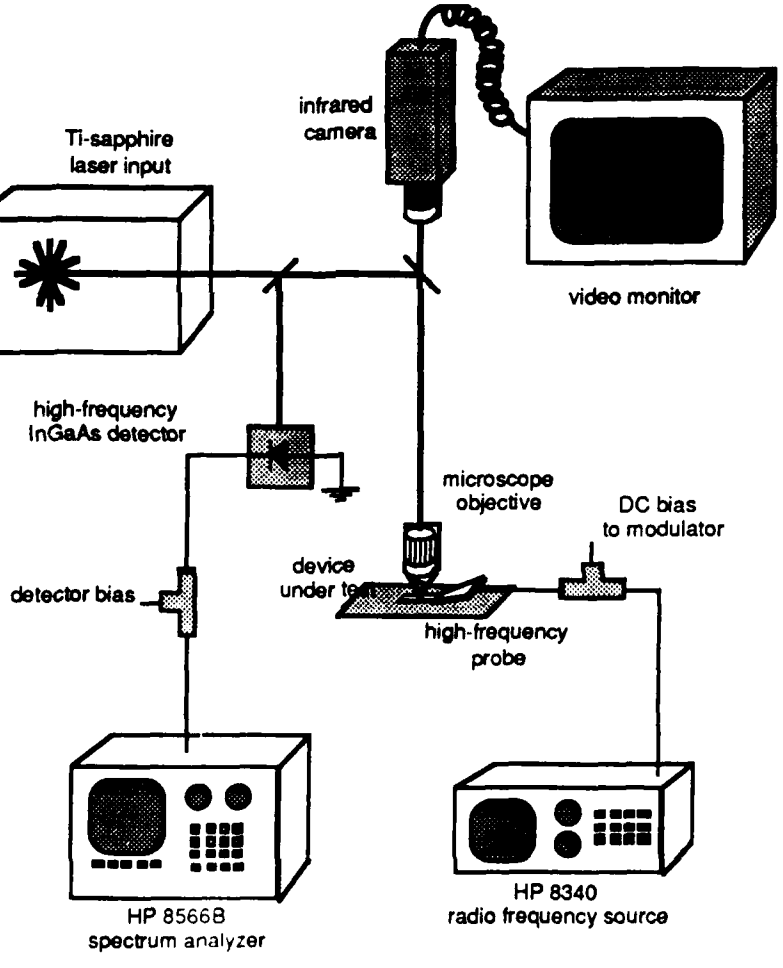

Figure IV-3

Optical Small-Signal Measurement Apparatus

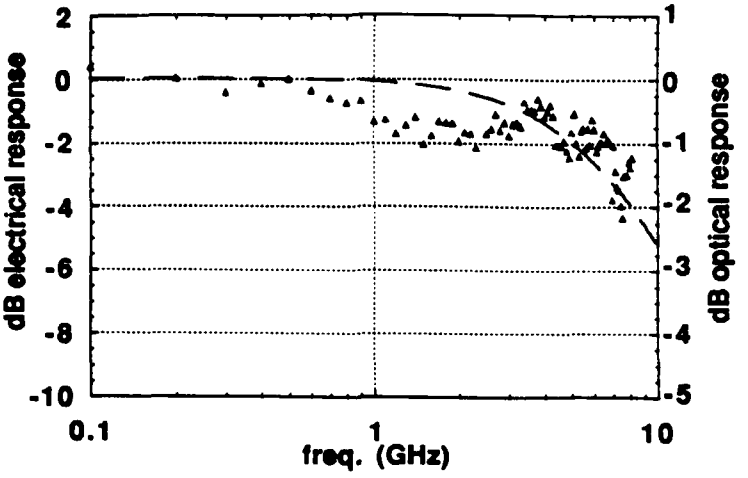

Figure IV-4.

(a) Measured and calculated optical response of a 42 x42 μm diode.
The electrical power in the detector is indicated on the lefthand scale.

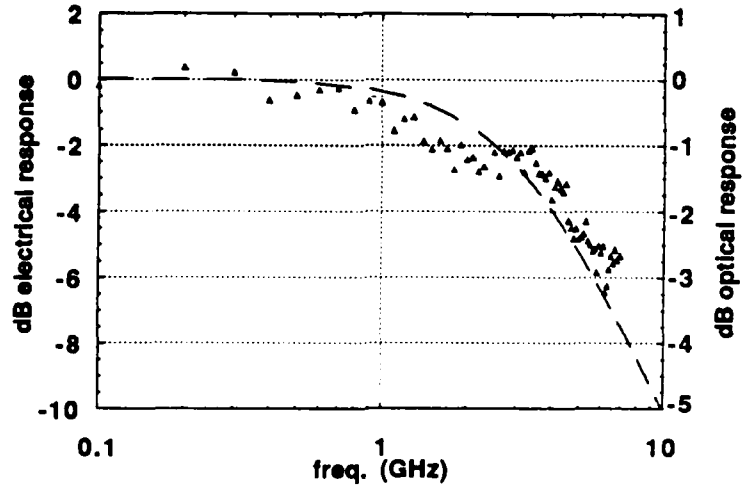

Figure IV-4

(b) Measured and calculated optical response of a 62 x62 μm diode.

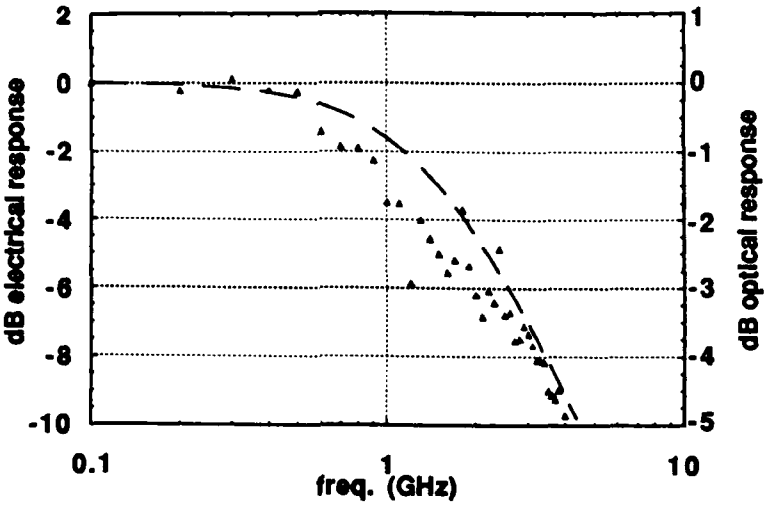

Figure IV-4.

(c) Measured and calculated optical response of a 102 x102 μm diode.

The performance of the modulator is sensitive to both bias and operating wavelength. The relative modulation efficiency (Figure IV-5) is fairly constant versus bias over a several-volt range, but is quite sensitive to the wavelength, as one would expect for a symmetric FP modulator.

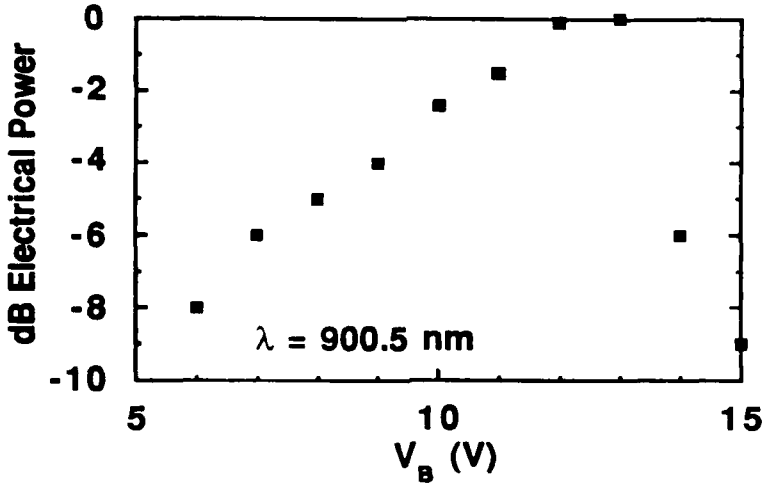

Figure IV-5

(a) Relative modulation efficiency at 100 MHz as a function of electrical bias for a 62 x 62 μm diode.

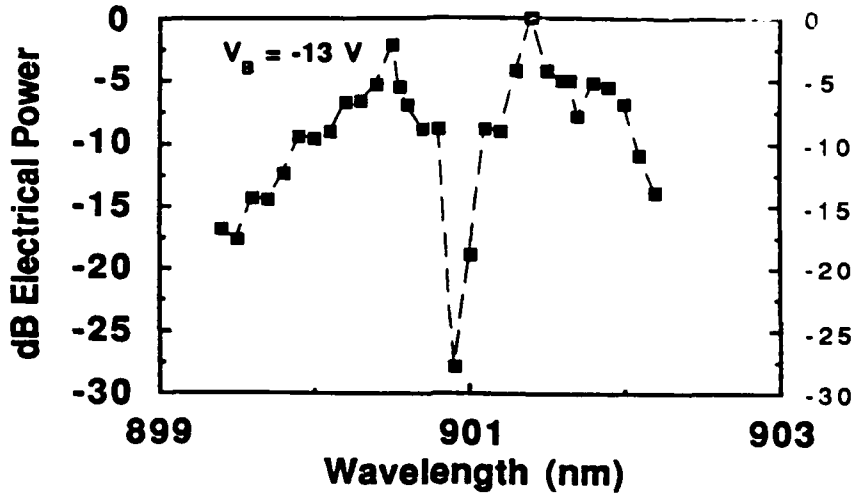

Figure IV-5

(b) Relative modulation efficiency at 100 MHz as a function of operating wavelength for a 62 x 62μm diode. We used a 4 dBm electrical signal for this measurement.

References

[1] T. H. Wood, "Multiple quantum well (MQW) waveguide modulators", *J. Lightwave Tech.* **6**, 743 (1988).

[2] R. H. Yan, R. J. Simes, L. A. Coldren, and A. C. Gossard, "Transvers modulators with a record reflection change of > 20 %/V using asymmetric Fabry-Perot structures", *Appl. Phys. Lett.* **56**, 1626 (1990).

[3] K-K Law, R. H. Yan, J. L. Merz, and L. A. Coldren, "Normally-off high-contrast asymmetric Fabry-Perot reflection modulator using Wannier-Stark localization in a superlattice", *Appl. Phys. Lett.* **56**, 1886 (1990).

[4] T. Y. Hsu, W. Y. Wu, and U. Efron, "Amplitude and phase modulation in a 4-μm-thick GaAs/AlGaAs multiple quantum well modulator", *Electron. Lett.* **24**, 603 (1988).

[5] G. D. Boyd, D. A. B. Miller, D. S. Chemla, S. L. McCall, A. C. Gossard, and J. H. English, "Multiple quantum well reflection modulator", *Appl. Phys. Lett.* **50**, 1119 (1987).

[6] R. B. Bailey, R. Sahai, and C. Lastufka, "1x16 arrays of GaAs/AlGaAs multiple quantum well optical modulators with 26:1 contrast", Optical Society of America, *Topical Meeting on Quantum Wells for Optics and Optoelectronics, 1989*, Paper PD-1 (Salt Lake City, Utah, 1989).

[7] R.J. Simes, R.H. Yan, R. S. Geels, L. A. Coldren, J. H. English, A. C. Gossard, and D. G. Lishan, "Electrically tunable Fabry-Perot mirror using multiple quantum well index modulation", *Appl. Phys. Lett.* **53**, 637 (1988).

[8] Y. H. Lee, J. L. Jewell, S. J. Walker, C. Tu, J. P. Harbison, and L. Tl Florez, "Electro-dispersive multiple-quantum-well modulator", *Appl. Phys. Lett.* **53**, 1684 (1988).

[9] R. H. Yan, R. J. Simes, and L. A. Coldren, "Analysis and design of surface-normal Fabry-Perot electro-optic modulators", IEEE *J. Quantum Electron.* **25**, 2272 (1989).

[10] R. H. Yan, R. J. Simes, and L. A. Coldren, "Electroabsorptive Fabry-Perot reflection modulator using asymmetric mirrors", IEEE *Photon. Tech. Lett.* **1**, 273 (1989).

[11] D. A. B. Miller, D. S. Chemla and S. Schmitt-Rink, "Electric field dependence of optical properties of semiconductor quantum wells", in *Optical Nonlinearities and Instabilities in Semiconductors*, H. Haug, ed., Academic, New York, 1988. (and the references therein).

[12] M. Whitehead and G. Parry, "Low-voltage multiple quantum well reflection modulator with on:off ratio > 100:1", *Electron. Lett.* **25**, 984-5 (1989).

[13] R. H. Yan, R. J. Simes, and L. A. Coldren, "Extremely low-voltage surface-normal reflection modulators", IEEE *Photon. Tech. Lett.* **2**, 118 (1990).

[14] H. A. Haus, *Waves and Fields in Optoelectronics*, Prentice-Hall, Englewood, NJ, 1984.

[15] R. H. Yan, K-K Law, L. A. Coldren, and J. L. Merz, "Asymmetric Fabry-Perot reflection modulator using red- and blue- shifted electro-absorption effects", *J. Appl. Phys.*, **68**, (2), 875-877, (1990).

[16] R. S. Geels, S. W. Corzine, J. W. Scott, D. B. Young, and L. A. Coldren, "Low threshold planarized vertical-cavity surface-emitting lasers", IEEE *Phot. Tech. Lett.* **2**, 234 (1990).

[17] M. A. Aframowitz, "Refractive Index of $Ga_{1-x}Al_xAs$", *Solid-State Communications* **15**, 59 (1974).

[18] R. H. Yan, R. J. Simes, and L. A. Coldren, "Wide-bandwidth, high-efficiency reflection modulators using an unbalanced Fabry-Perot structure", *Appl. Phys. Lett.* **55**, 1946 (1989).

[19] R. H. Yan and L. A. Coldren, "Effect of temperature on the operating characteristics of asymmetric Fabry-Perot reflection modulators", *Appl. Phys. Lett.*, **57**, (3), 267-269, (1990).

[20] R.H. Yan, R.J. Simes, H. Ribot, L.A. Coldren and A.C. Gossard, "Blue-Shifted Absorption using Field-Induced Stark Localization in Superlattices," *CLEO '89*, MJ4, Baltimore, MD, (April 1989).

[21] J. Bleuse, G. Bastard and P. Voisin, *Phys. Rev. Lett.* **60**, 220 (1988); J. Bleuse, P. Voisin, M. Allovon and M. Quillec, *Appl. Phys. Lett.* **53**, 2632 (1988); E. E. Mendez, F. Agullo-Rueda and J. M. Hong, *Phys. Rev. Lett.*, **60**, 2426 (1988).

[22] K-K. Law, R.H. Yan, J.L. Merz, and L.A. Coldren, "Normally-Off High-Contrast Asymmetric Fabry-Perot Reflection Modulators Using Wannier-Stark Localization in Superlattices," *Applied Physics Lett.*, **56**, 1886, (May 7, 1990).

[23] D. A. B. Miller, D. S. Chemla, T. C. Damen, T. H. Wood, C. A. Burrus, Jr., A. C. Gossard and W. Wiegmann, "The quantum well self-electro-optic effect device: Optoelectronic bistability and oscillation, and self-linearized modulation", *IEEE J. Quantum Electron.*, **QE-21**, 1462 (1985).

[24] D. A. B. Miller, J. E. Henry, A. C. Gossard and J. H. English, "Integrated quantum well self-electro-optic effect device: 2x2 array of optically bistable devices", *Appl. Phys. Lett*, **49**, 821 (1986).

[25] A. L. Lentine, H. S. Hinton, D. A. B. Miller, J. E. Henry, J. E. Cunningham And L. M. F. Chirovsky, "Symmetric self-electro-optic effect device: Optical set-reset latch", *Appl. Phys. Lett*, **53**, 1419 (1988).

[26] K-K. Law, R.H. Yan, L.A. Coldren, and J.L. Merz, "A Self-electro-optic device based on a superlattice asymmetric Fabry-Perot modulator with an on/off ratio >100:1," *Applied Phyics. Lett.*, **57**, (13), 1345-1347, (September 24, 1990).

V. Conference and Journal Publications

[1] "Blue-Shifted Absorption using Field-Induced Stark Localization in Superlattices," R.H. Yan, R.J. Simes, H. Ribot, L.A. Coldren and A.C. Gossard, *CLEO '89*, MJ4, Baltimore, MD, (April 1989).

[2] "Electro-Absorptive Fabry-Perot Reflection Modulators with Asymmetric Mirrors," R.H. Yan, R.J. Simes, and L.A. Coldren, *IEEE Photonics Technol. Lett.*, **1**, (9) 273-275, (September 1989).

[3] "Multiple Quantum Well Asymmetric Fabry-Perot Reflection Modulators," R.H. Yan, R.J. Simes and L.A. Coldren, *IEEE LEOS '89*, OE3.2, Orlando, FL, (October 1989).

[4] "Analysis and Design of Surface-Normal Fabry-Perot Electro-Optic Modulators," R.H. Yan, R.J. Simes, and L.A. Coldren, *IEEE J. Quantum Electron.*, **25**, pp. 2272-2280, (November 1989).

[5] "Wide-Bandwidth, High-Efficiency Reflection Modulators Using an Unbalanced Fabry-Perot Structure," R.H. Yan, R.J. Simes, and L.A. Coldren, *Applied Physics Lett.*, **55**, (19), 1946-1948, (November 6, 1989).

[6] "Extremely Low-Voltage Fabry-Perot Reflection Modulators", R.H. Yan, R.J. Simes, L.A. Coldren, *IEEE Photonics Technol. Lett..*, **2**, (2), (February 1990).

[7] "Transverse Modulators with a Record Reflection Change of >20%/V Using Asymmetric Fabry-Perot Structures," R.H. Yan, R.J. Simes, L.A. Coldren, and A.C. Gossard, *Applied Physics Lett.*, **56**, (17), 1626-1628 (April 23, 1990).

[8] "Normally-Off High-Contrast Asymmetric Fabry-Perot Reflection Modulators Using Wannier-Stark Localization in Superlattices," K-K. Law, R.H. Yan, J.L. Merz, and L.A. Coldren, *Applied Physics Lett.*, **56**, 1886, (May 7, 1990).

[9] "Superlattice Asymmetric Fabry-Perot Reflection Modulator," K-K. Law, R.H. Yan, L.A. Coldren and J.L. Merz, *CLEO'90*, paper no. CTUC3, Anaheim, CA, (May, 1990).

[10] "A Self-Electro-Optic Effect Device Using Superlattice Asymmetric Fabry-Perot Modulators", K-K. Law, R.H. Yan, L.A. Coldren and J.L. Merz, *1990 Device Research Conference*, paper VIB-4, Santa Barbara, CA, (June 1990).

[11] "Surface-Normal Electro-Absorption Reflection Modulators Using Asymmetric Fabry-Perot Structures,"
R.H. Yan, R.J. Simes, and L.A. Coldren,
IEEE J. Quantum Electron., (To be published July 91).

[12] "Asymmetric Fabry-Perot Reflection Modulators Using Red- and Blue-Shifted Electroabsorption Effects,"
R.H. Yan, K.K. Law, L.A. Coldren, and J.L. Merz,
J. Applied Physics, **68**, (2), 875-877, (July 15, 1990).

[13] "Effect of Temperature on the Operating Characteristic of Asymmetric Fabry-Perot Reflection Modulators,"
R.H. Yan and L.A. Coldren,
Applied Physics Lett., **57**, (3), 267-269, (July 16, 1990).

[14] "Self-Electro-Optic Effect Device Based on an Asymmetric Fabry-Perot Modulator Using Wannier-Stark Localization in Superlattice,"
K.K. Law, R.H. Yan, L.A. Coldren, and J.L. Merz,
NLO (Nonlinear Optics) '90, Kauai, Hawaii, paper no. TP15, (July 16 - 20, 1990).

[15] "A Self-electro-optic device based on a superlattice asymmetric Fabry-Perot modulator with an on/off ratio >100:1,"
K-K. Law, R.H. Yan, L.A. Coldren, and J.L. Merz,
Applied Phyics. Lett., **57**, (13), 1345-1347, (September 24, 1990).

[16] "High-Frequency electro-optic Fabry-Perot Modulator,"
R.J. Simes, R.H. Yan, C.C. Barron, D. Derickson, D.G. Lishan, J. Karin, L.A. Coldren and M. Rodwell,
IEEE Photonics Technol. Lett., (To be published June 1991).

[17] "High-Efficiency Vertical-Cavity Surface-Emitting Lasers and Modulators,"
(INVITED PAPER)
L.A. Coldren,
SPIE'90, 1362, Aachen, Germany, (October 28 - November 2, 1990),

[18] "High Performance Fabry-Perot Transverse Optical Modulators," (INVITED PAPER)
L.A. Coldren and R.H. Yan,
LEOS'90, Boston, MA, paper no. OE7.1, (November 4-9, 1990).

[19] "Optical modulation and switching using GaAs/AlGaAs Superlattice Asymmetric Fabry-Perot Modulator grown by MBE,"
K-K. Law, R.H. Yan, J.L. Merz and L.A. Coldren,
European MRS'90, Strasbourg, France, Paper no. A-12.5, (November 27-30, 1990).

[20] "Measurement of field-induced refractive index variation in a GaAs/AlGaAs superlattice using a monolithic Fabry-Perot etalon,"
K-K. Law, R.H. Yan, L.A. Coldren and J.L. Merz,
Electronics Letters, **27**, No.2, pp. 105-106 (Jan 17 1991)

[21] "High-contrast Fabry-Perot Electroabsorption Modulators," (INVITED PAPER)
R-H. Yan, R.J. Simes, and L.A. Coldren,
Quantum Optoelectronics Topical Meeting, paper no. MB1-1, Salt Lake City, UT, (March 11-13, 1991).

[22] "Large excitonic blue-shift and nonlinearity in narrow asymmetric coupled quantum wells,"
Y.J. Ding, C.L. Guo, S. Li, J.B. Khurgin, K-K. Law, J. Stellato, C.T. Law, A.E. Kaplan and L.A. Coldren,
Quantum Optoelectronics Topical Meeting, Paper no. MD6-1, Salt Lake City, UT, (March 11-13, 1991).

VI. Personnel

Professor Larry A. Coldren, Ph.D.: Principal Investigator
Dr. Coldren received his doctorate from Stanford University in 1972. He spent the next twelve years at AT&T Bell Labs before moving to the University of California at Santa Barbara in 1984. He holds 25 patents in the areas of surface-acoustic-wave signal processing devices, microfabrication processes and III-V optoelectronic devices for optical communications and processing. He has over 190 journal publications in these same areas. His current interests are in the areas of components for optical communication, optical computing and microfabrication technology.

Dr. R.J. Simes: (former) Graduate Student Researcher
Rob Simes received a B.S. with highest honors from UCSB in December, 1983 and started graduate studies immediately thereafter. His contributions to this work include molecular beam epitaxy of surface-normal optoelectronic structures, and their fabrication and testing. He completed his Ph.D. in June, 1990, and is currently with Alcatel-Alsthom Recherche in Paris, France.

Dr. R.H. Yan: (former) Graduate Student Researcher
Ran-Hong Yan received his B.S. degree from National Taiwan University in 1984 and came to UCSB in 1986. His contributions to this research included both theoretical optimization of Fabry-Perot structures and device testing. He also completed his Ph.D. in 1990, having authored or co-authored more than 40 technical papers, and has since joined AT&T Bell Labs in Holmdel, N.J.

Mr. K.K. Law: Graduate Student Researcher
Kwok-Keung Law received the B.Sc.(Hons) from the Chinese University of Hong Kong. He worked for the Hong Kong Telephone Company as a telecommunication engineer for three years before he joined UCSB for graduate study. Currently he is working towards the Ph.D. degree with interest focused on the optoelectronic devices with vertical cavity structures for optical communication and computing, and molecular beam epitaxy.

Ms. C.C. Barron: Graduate Student Researcher

Carole Craig Barron received a B.S. with highest honors in Electrical and Computer Engineering and a B.A. with highest honors in the Liberal Arts from the University of Texas at Austin in 1988. She began working with Prof. Coldren in the spring of 1989, and completed her M.S. at UCSB in December of that year. She is currently concentrating on the design and fabrication of extremely high-speed Fabry-Perot modulators.

Dr. M. Whitehead: Visiting Research Engineer

Mark Whitehead received the B.Sc. degree from Imperial College, University of London, England, in 1984. From 1984 to 1985 he worked as an Associate Research Assistant at University College London, England on a project to investigate GaAs-AlGaAs multiple quantum well optical modulators. During the period 1985-1988 he was enrolled in the Ph.D. program at University College, working on the same project. He took up a position as a Post-doctoral Research Assistant in 1988 at the same establishment, and it was during this period that he proposed and demonstrated the first multiple quantum well asymmetric Fabry-Perot modulator. In 1990 he received the Ph.D. degree from University College. He moved to the University of California Santa Barbara, in May of 1990, in order to take up a posit;ion as a Visiting Research Engineer, working on the optimization of surface normal resonant cavity modulators.